Journal of Catalysis **210,** 295–312 (2002)
doi:10.1006/jcat.2002.3675

Adsorption Characteristics of Sol-Gel Gd–Pd/TiO_2 Catalysts in Reduction of Nitric Oxide with CH_4: DRIFTS and TPD

Junko M. Watson and Umit S. Ozkan[1]

Department of Chemical Engineering, The Ohio State University, Columbus, Ohio 43210

Received January 10, 2002; revised May 10, 2002; accepted May 17, 2002

Palladium and gadolinium–palladium catalysts supported on titania were studied for the catalytic reduction of NO by CH_4. *In situ* diffuse reflectance infrared Fourier transform spectroscopy (DRIFTS) was used to identify adsorbed species under NO, NO + CH_4, and NO + CH_4 + O_2 flows. NO adsorption resulted in formation of various nitrogen-oxo adspecies such as bridged/bidentate nitrate, monodentate nitrate, nitro, and linear NO. The thermal stability of these species is examined and related to the NO desorption features observed in temperature-programmed-desorption profiles. Even at room temperature, CH_4 was found to adsorb on the surface and hinder the NO adsorption. The Pd^0 sites were essential for dissociative adsorption of methane. Under conditions where the catalyst was fully active for NO reduction, NH_3 was seen to form as molecularly adsorbed species on Lewis acid sites. It appears that hydrogen abstraction from methane is a prerequisite for the formation of NH_x species, which are believed to act as a reducing agent for adsorbed NO, although direct interaction of nitro/nitroso species with surface CH_x remains a possibility. The Gd addition was found to change the catalytic chemistry significantly, possibly due to its high electropositivity, which helps stabilize the electron density at the Pd sites.

Key Words: **nitric oxide reduction; methane; palladium; DRIFTS; TPD.**

INTRODUCTION

Although there is an established technology for the selective catalytic reduction (SCR) of nitric oxide that is based on ammonia, there are lingering environmental and economic concerns regarding use of ammonia as a reducing agent. In the use of hydrocarbons as alternative reducing agents, in particular, methane has attracted much attention because it is the most abundant and least expensive hydrocarbon in natural gas. Activation of methane is the most difficult among hydrocarbons since it is the most stable molecule among alkanes. There is a large volume of literature on different catalysts that have been investigated for the catalytic reduction of NO with methane in the presence of oxygen including metal-exchanged zeolitic catalysts such as Co/ZSM-5 (1–3), Pd-H-ZSM-5, and Pd-Ce-H-ZSM-5 (4–6). A group of nonzeolitic catalysts (La_2O_3, CeO_2, Nd_2O_3, Sm_2O_3, Tm_2O_3, and Lu_2O_3) was studied by Vannice and co-workers (7, 8). Noble metals such as Pd, Pt, and Rh supported on silica and/or alumina were also investigated for NO–CH_4 reaction with and without the presence of oxygen (9–11), including a smaller number of studies that focused on the use of titania-supported palladium. Ueda *et al.* studied the reduction of NO using hydrogen in the presence of oxygen and water vapor (12). We reported the effective use of Pd-based catalysts supported on titania for the NO reduction with methane in the presence of oxygen (13–18). The extent of the reaction was found to be highly dependent on the palladium oxidation state, and the metallic phase of palladium was found to be necessary for the reduction of NO to N_2.

In situ FTIR spectroscopy is a powerful tool which has been extensively used to help elucidate reaction mechanisms. Over Co-FER, Li and Armor (19) used diffuse reflectance infrared Fourier transform spectroscopy (DRIFTS) to elucidate possible mechanisms in the NO–CH_4–O_2 reaction. According to their proposed mechanism, formation of adsorbed NO_2 on Co^{2+} sites is the first step, followed by CH_4 activation by the adsorbed NO_2, forming $CH_3^{\bullet}$ radicals. The $CH_3^{\bullet}$ radical could react with adsorbed NO_2 to form nitromethane (CH_3NO_2) which can react further with gas-phase NO to form N_2, H_2O, and CO_2 (19). Hall and co-workers studied the role of free $CH_3^{\bullet}$ radicals over Co-ZSM-5 and H-ZSM-5 catalysts and proposed that after the oxidation of NO to NO_2, $CH_3^{\bullet}$ free radicals react with NO_x and O_2 (20).

The rate-determining step in the NO–CH_4–O_2 reaction was shown to be the breaking of the C–H bond on Co-ZSM-5 catalysts (9, 21). But there was no dominant rate-determining step in the NO–CH_4–O_2 reaction over a Pd-H-ZSM-5 catalyst. The values obtained for N_2 formation by using kinetic isotope effects, k_H/k_D, were smaller than the values reported in the case of Co-ZSM-5, suggesting that the C–H cleavage may be one of the many rate-determining steps. However, it was demonstrated that the oxidation of

[1] To whom correspondence should be addressed. E-mail: Ozkan.1@osu.edu.

0021-9517/02 $35.00

NO became the rate-controlling step at low temperatures (21, 22).

Using *in situ* IR spectroscopy, Lobree *et al.* observed Co^{2+}–CN and Al^{3+}–NCO species during NO reduction with CH_4 over a Co-ZSM-5 catalyst. The reaction rate of CN species was determined to be faster in the presence of NO_2 than it was with O_2 or NO; therefore, the CN species were considered to be reaction intermediates. Possible mechanistic steps over Co-ZSM-5 included formation of surface nitrosomethane (CH_3NO) (23).

Over an Mn-ZSM-5 catalyst, Mn^{2+} is slowly oxidized to Mn^{3+} by NO adsorption and simultaneously, $Mn^{2+}(NO)$ and $Mn^{3+}(O^{\cdot})(NO)$ species are formed. Again, CN species were reported to form and were shown to react rapidly with NO_2 (24). However, other researchers proposed that methyl species combined directly with adsorbed NO_2 to form nitromethane (CH_3NO_2). A mechanistic study of the NO–CH_4–O_2 reaction over Co-ZSM-5 was also conducted by Sun *et al.* using DRIFTS. The presence of O_2 enhanced NO oxidation to form adsorbed NO_2. The authors suggested that the adsorbed NO_2 could react with methane to generate nitromethane intermediates (25).

Also, over M-ZSM-5 (M = Co, H, Fe, Cu), Hall and coworkers investigated the role of nitromethane in NO reduction with CH_4 in the presence of excess O_2 where $^{15}N^{18}O$ was used as a tracer to react with CH_3NO_2 to determine the origin of the nitrogen product. They found that the predominant N_2 was $^{15}N^{14}N$ indicating that an N atom from both $^{15}N^{18}O$ and CH_3NO_2 is utilized in the formation of molecular nitrogen (26).

Ozkan and co-workers studied the mechanistic aspects of NO–CH_4 reactions using isotopic labeling techniques under both steady-state and transient conditions. From a series of unsteady-state and steady-state isotopic labeling studies that used various labeled species such as $^{15}N^{16}O$, $^{15}N^{18}O$, $^{13}CH_4$, and $^{18}O_2$, it was concluded that N_2 was formed through direct participation of CH_4, possibly through a methyl-nitrosyl-type intermediate, whereas N_2O formation was mainly a result of an NO decomposition reaction (14). Also, steady-state oscillations were used as a probe to gain insight into the reaction network and found that the oxidation state of the active metal determined the extent of the three different reaction steps, namely, NO reduction with CH_4, direct CH_4 oxidation, and NO decomposition (15).

In this paper, we present the second phase of our studies that examine the surface species in the NO–CH_4–O_2 reaction with *in situ* DRIFTS where the first phase was reported in a previous paper (27). We used temperature-programmed desorption (TPD) and *in situ* DRIFTS to determine the nature of the adsorbed species under reaction conditions on Pd/TiO_2 and Gd–Pd/TiO_2. Using the information obtained, mechanistic implications in the NO–CH_4–O_2 reaction over Pd/TiO_2 and Gd–Pd/TiO_2 catalysts are discussed.

METHODS

Catalyst Preparation

Catalysts were synthesized using a modified sol-gel technique in which co-precipitation and sol-gel methods are incorporated as described elsewhere (18). The metal loadings of the catalysts were 2% Pd/TiO_2 and 1% Gd–2% Pd/TiO_2 by weight percentage. The BET surface area measurement by N_2 adsorption resulted in the specific surface areas of 30 m^2/g, 51 m^2/g, and 62 m^2/g for TiO_2, 2% Pd/TiO_2 and 1% Gd–2% Pd/TiO_2, respectively. Catalysts which are denoted as "reduced" were pretreated with hydrogen (33% in He, 30 cm^3/min flow rate) for 30 min at 200°C.

Catalyst Characterization

Temperature-programmed-reduction (TPR) experiments were performed using a TPR/TPD flow system equipped with a thermal conductivity detector (TCD). A U-tube quartz reactor with 0.25-in. o.d. was packed with 150 mg of sample using quartz wool at the top and the bottom of the catalyst bed. The catalyst was calcined *in situ* in 10% O_2 in balance He for 1 h at 500°C followed by cooling under N_2 to room temperature. After the sample was cooled to room temperature, it was further cooled to −50°C by flowing air that was chilled in liquid N_2 around the reactor. The reduction was performed with 10% H_2 in balance N_2 at 25 cm^3(STP)/min. The water vapor produced during the reduction was removed by passing the outlet flow through a column of silica gel before reaching the TCD. The temperature program during the reduction was 5 min at −15°C, 10°C/min ramping to 850°C, and 5 min at 850°C.

TPD experiments were conducted using the same TPR/TPD system described earlier and the desorption species were monitored by an HP5890GC-MS. The sample (75 mg) was loaded into the U-shaped quartz reactor and calcined *in situ* in 10% oxygen in balance helium at 500°C for 30 min followed by flushing in helium for 30 min. Then the sample was reduced in 33% hydrogen in balance helium at 200°C for 30 min followed by flushing for 30 min in helium. Then the catalyst was cooled down to room temperature under helium flow. Adsorption was performed at room temperature for 1 h followed by helium flushing for 1 h to remove physically adsorbed gas.

DRIFTS experiments were performed using a Bruker IFS66 equipped with a DTGS detector and a KBr beamsplitter. Catalysts were placed in a sample cup inside a Spectratech diffuse reflectance cell equipped with KBr windows and a thermocouple mount that allowed direct measurement of the surface temperature. Each catalyst was pretreated *in situ* either by calcination under 10% oxygen at 400°C surface temperature or by reduction under

30% hydrogen in balance helium at 200°C surface temperature for 30 min. Background spectra were taken after pretreatment at each temperature level. For sequential adsorption at 300°C surface temperature, background spectra were taken at 300°C under helium before adsorption gases were introduced. For adsorption spectra obtained at several different temperature levels, background spectra were taken at each temperature level under helium prior to the introduction of adsorption gas. Each spectrum was averaged over 1000 scans in the mid-IR range (400–4000 cm^{-1}) to a nominal 2 cm^{-1} resolution.

RESULTS

TPR

TPR experiments on oxidized 2% Pd/TiO_2 and 1% Gd–2% Pd/TiO_2 were performed using 10% H_2/He as a reducing agent. While there were two distinct hydrogen consumption peaks observed on the Pd-only catalyst at 15°C and 31°C, the lower-temperature feature was not observed on the Gd–Pd sample (Fig. 1). This suggests that there is a second reduction site over the Pd-only catalyst which does not exist over the Gd-containing catalyst.

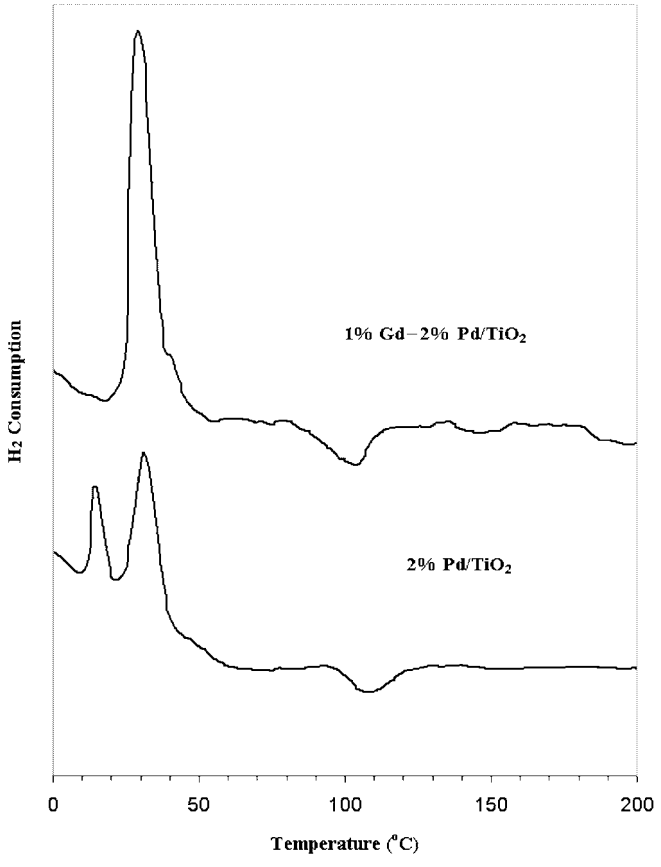

FIG. 1. H_2 TPR profiles of oxidized 1% Gd–2% Pd/TiO_2 and 2% Pd/TiO_2.

In addition to the temperature maxima observed below 50°C, there was a broad hydrogen evolution feature, i.e., a negative peak, over both catalysts at 108°C indicating the Pd-based catalysts on titania can adsorb/absorb hydrogen in the surface/bulk at lower temperatures and release molecular hydrogen at higher temperatures, suggesting the formation and subsequent decomposition of a hydride.

XPS

Pd 3d XPS spectra were taken on the reduced and oxidized Pd/TiO_2 and Gd–Pd/TiO_2 samples to determine the oxidation states of Pd and to help explain the TPR results. The catalyst reduction was performed in a mixture of 33% H_2 in He for 30 min at 200°C and transferred to the XPS chamber without exposure to the atmosphere. The Pd $3d_{5/2}$ and Pd $3d_{3/2}$ peaks at zero oxidation state are present at 334.1 and 339.5 eV, respectively. The completely oxidized catalyst gave Pd $3d_{5/2}$ and Pd $3d_{3/2}$ peaks at 335.3 and 340.5 eV, respectively. On the reduced Pd/TiO_2 catalyst, Pd was found to exist in both oxide and metallic phases. The deconvolution of these peaks showed palladium to be primarily in zero oxidation state (79% and 84% for Pd and Gd–Pd, respectively) in the reduced samples (Fig. 2 curves a and b). In Fig. 2 (curve c), the Pd 3d spectrum over the oxidized Gd–Pd catalyst showed single peaks at 335.8 and 341.1 eV for Pd $3d_{5/2}$ and Pd $3d_{3/2}$, respectively. This indicates that, prior to reduction, all Pd on the surface was in 2+ oxidation state over the Gd–Pd catalyst.

Figure 2 (curve d) is the Pd 3d spectrum of the oxidized Pd-only catalyst which, in addition to the feature that corresponds to Pd^{2+}, exhibits a shoulder at a higher binding energy. After deconvolution, two peaks are observed at 335.7 and 336.9 eV for Pd $3d_{5/2}$ and 340.9 and 342.2 eV for Pd $3d_{3/2}$. The peak at the lower binding energy corresponding to PdO makes up 45% of total Pd on the surface. The additional peak at the higher binding energy can be assigned to Pd in 4+ oxidation state.

The fact that an additional oxidation state of Pd was observed for the Pd-only catalyst seems to support the H_2-TPR results, in which two distinct reduction features were observed over the Pd-only catalyst. The hydrogen consumption at the lower temperature, therefore, is associated with the reduction of PdO_2 species.

TPD

NO adsorption. TPD using NO was performed over sol-gel TiO_2, Pd/TiO_2, and Gd–Pd/TiO_2. The samples were reduced *in situ* with 33% H_2 in He at 200°C, followed by NO adsorption at room temperature for 1 h using a stream of 5000 ppm NO in He at a flow rate of 25 cm^3 (STP)/min. The system was flushed with He prior to starting the linear temperature program. NO was seen to adsorb both reversibly and irreversibly (Fig. 3, plots a and b). The NO desorption profiles ($m/e = 30$) for sol-gel TiO_2, Pd/TiO_2, and

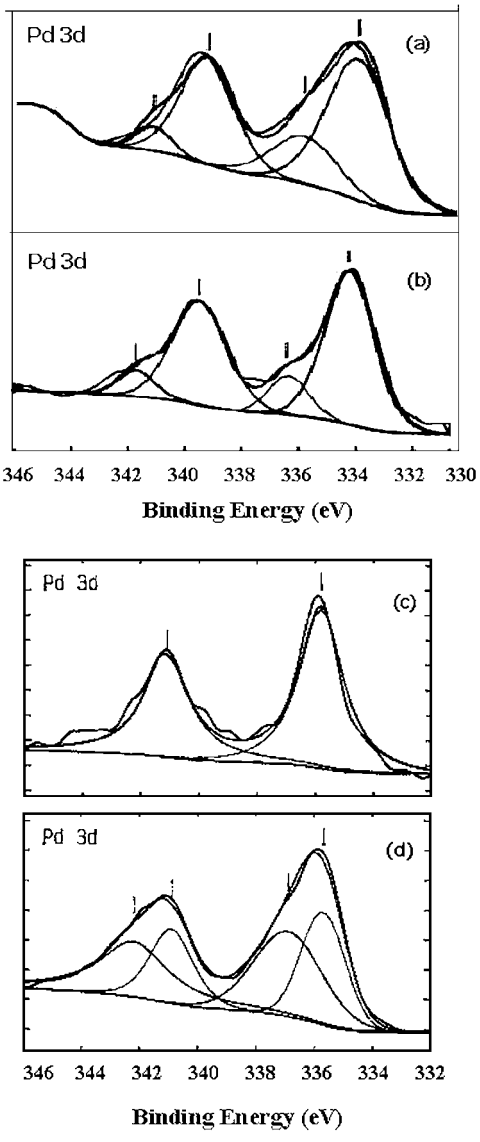

FIG. 2. X-ray photoelectron spectra of reduced (a) 2% Pd/TiO_2, (b) 1% Gd–2% Pd/TiO_2, and oxidized (c) 1% Gd–2% Pd/TiO_2, (d) 2% Pd/TiO_2.

Gd–Pd/TiO_2 are shown in Fig. 3 (plot a). The NO desorption profile for the sol-gel TiO_2 in the temperature range between 50 and 500°C consists of a small peak around 150°C. Over Pd/TiO_2, there are two NO desorption features at 126 and 182°C. In the presence of Gd, there was a new peak observed at 275°C in addition to those observed over the Gd-free catalyst. The reversible NO adsorption capacity was significantly increased over Gd–Pd/TiO_2 compared to Pd/TiO_2, suggesting that the synthesis involving Gd enhanced the number of NO adsorption sites.

In addition to NO desorption, N_2O ($m/e = 44$) and N_2 ($m/e = 28$) were also seen to desorb on Gd–Pd/TiO_2 (Fig. 3, plot b), suggesting that NO decomposition/coupling took place on this catalyst. The lowest- and highest-temperature features of the Gd–Pd catalyst coincided with N_2 and N_2O desorption features. There was no significant desorption of N_2 or N_2O for Pd-only catalyst. An oxygen desorption peak for the Gd–Pd catalyst was observed at 610°C. The oxygen desorption was expected since dissociation of NO occurred. Interestingly, there was no low-temperature O_2 desorption coinciding with the N_2 and N_2O features, suggesting that the oxygen from the NO decomposition could be consumed for reoxidation of the Pd sites or absorbed into the bulk, as reported in the literature (28, 29), and released at higher temperatures. Sharpe *et al.* also observed a similar result when NO was adsorbed on Pd(110) (28). A control experiment in which the catalyst was exposed to the same temperature program without an adsorption step was performed to determine the source of oxygen evolving from the surface. Although lower in intensity, the O_2 profile obtained in this blank TPD experiment also showed a desorption feature at 630°C, suggesting that oxygen could also originate from the catalyst matrix. It is conceivable that, while NO adsorption/decomposition increases the available oxygen that could be released from the surface, independent of

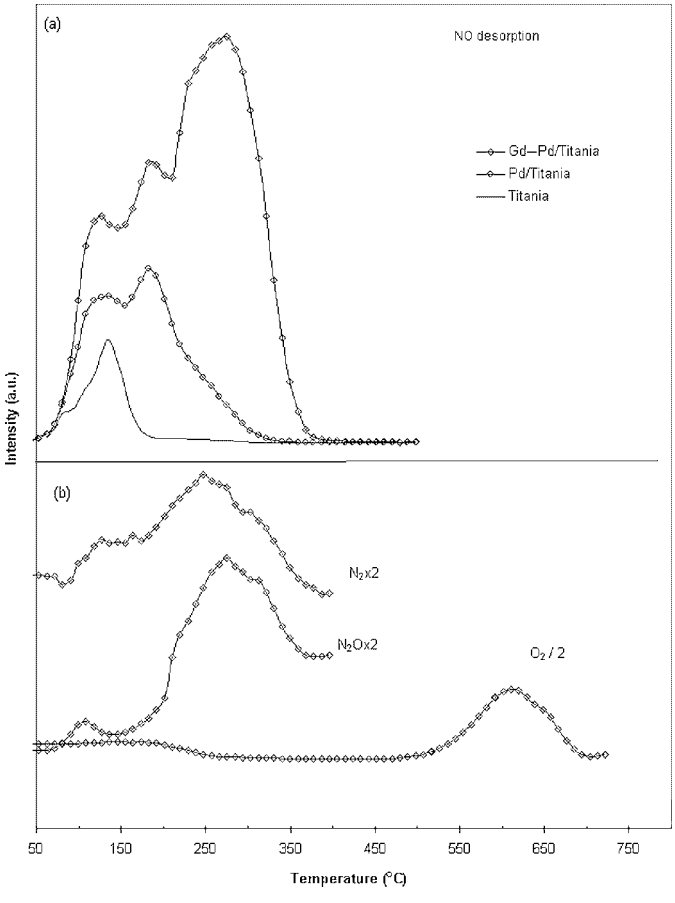

FIG. 3. Desorption profiles for NO TPD: (a) NO desorption profiles for TiO_2, Pd/TiO_2, and Gd–Pd/TiO_2; (b)N_2, N_2O, and O_2 desorption profiles for Gd–Pd/TiO_2.

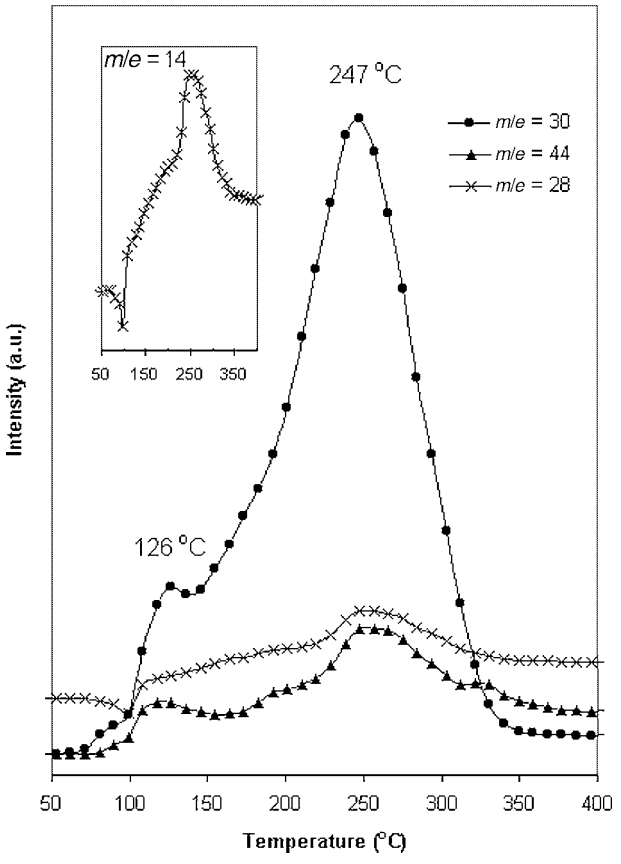

FIG. 4. TPD of co-adsorbed NO and CH_4 on reduced Pd/TiO_2.

this process, the catalyst and/or the support could also have oxygen that is labile enough to evolve from the surface at higher temperatures. There have been reports in the literature referring to increased oxygen mobility observed in titania when precious metals are supported over it (30, 31).

$NO + CH_4$ co-adsorption. To examine the competitive adsorption effects between NO and CH_4 and to assess how the adsorption sites could be affected through this competition, these two reactants were co-adsorbed on catalyst surfaces. The TPD profiles for the co-adsorption experiments for the Pd/TiO_2 and $Gd–Pd/TiO_2$ catalysts are shown in Figs. 4 and 5, respectively. After the catalyst was reduced *in situ*, a mixture of 1200 ppm NO and 7900 ppm CH_4 in He was introduced to the system at room temperature. After 1 h of co-adsorption, the catalyst was flushed with He for an additional hour and then the temperature program was initiated under He at 10°C/min.

The signal traces of $m/e = 30$, 44, and 28 were used to follow the desorption of NO, N_2O, and N_2, respectively. The signal for $m/e = 14$ could result from fractionation of all nitrogen-containing species. Though $m/e = 44$ and 28 could also result from CO_2 and CO desorption, respectively, one could use the curve shape of $m/e = 14$ to distinguish N_2 from CO and N_2O from CO_2. If the profile of $m/e = 14$ follows a similar trend in $m/e = 44$ or 28, we could qualitatively assign it to desorption of the nitrogen-containing species. When NO desorption profiles for Pd/TiO_2 in Fig. 3 (after NO adsorption) and Fig. 4 (after NO + CH_4 adsorption) were compared, there was an additional strong feature at 247°C which appeared only when NO and CH_4 were co-adsorbed. Concurrently, the $m/e = 28$ and 44 signals had a maximum at 247°C.

The NO desorption profile for $Gd–Pd/TiO_2$ after co-adsorption (Fig. 5) showed only one peak at 139°C, eliminating the higher-temperature desorption features that were observed after NO exposure. Over the Gd–Pd catalyst, the $m/e = 28$ signal gave two major peaks at 139 and 289°C where the second peak had a much higher intensity. Although CO could contribute to the $m/e = 28$ signal, since the profiles for $m/e = 14$ and 28 were very similar, it is more likely that this profile was due to N_2 desorption. Also, in the temperature range over which desorption peaks of 28 and 44 were detected, we observed desorption of H_2O (figure not shown). Since our blank TPD experiments, which are performed without an adsorption step, showed no water desorption from the surface, the water observed

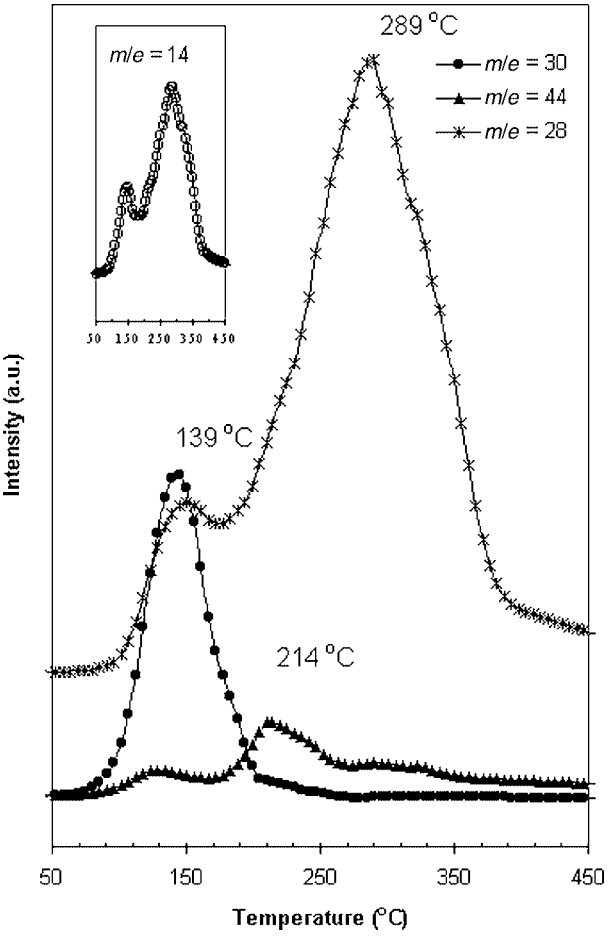

FIG. 5. TPD of co-adsorbed NO and CH_4 on reduced $Gd–Pd/TiO_2$.

in this experiment was likely due to reaction of CH_4. This implies involvement of CH_4 in the reduction/coupling reaction of NO adsorbed at the mid- and high-temperature sites, leading primarily to N_2 formation. Subsequently, it also suggests that even at room temperature, CH_4 can irreversibly adsorb on the catalyst surface.

Sequential CH_4/NO adsorption. The effect of preadsorbing CH_4 on NO adsorption sites was studied on reduced Gd–Pd/TiO_2 and the resulting TPD profiles for $m/e = 30$, 44, and 28 are shown in Fig. 6. After *in situ* reduction of the catalyst, 10% CH_4 in He was introduced to the system followed by He flushing. Next, 0.5% NO in He was adsorbed at room temperature. The NO desorption profile was similar to Fig. 5 where NO and CH_4 were co-adsorbed and where the mid- and high-temperature features were absent. This is additional evidence that methane may be adsorbed strongly and competitively with NO over the mid- and high-temperature sites. The desorption profiles for $m/e = 44$ and 28, however, were significantly different from Fig. 5. In this case, the strong N_2 desorption feature was completely missing, suggesting that CH_4 could be blocking the sites and making fewer sites available for NO to adsorb and subsequently react through a NO(ad)–CH_4(ad) reaction. Since this experiment does not differentiate between CO_2 and N_2O, we ran a similar experiment using the labeled species $^{13}CH_4$ and ^{15}NO. The adsorption time was considerably shorter in order to minimize the use of labeled gases. The desorption profiles for CO_2 and N_2O are shown in Fig. 6b. This figure clearly shows formation and desorption of CO_2 at three different temperatures. This result is significant in showing that CH_4 not only adsorbs strongly on the surface, but is also capable of reacting with oxygen from the catalyst surface and/or NO molecule.

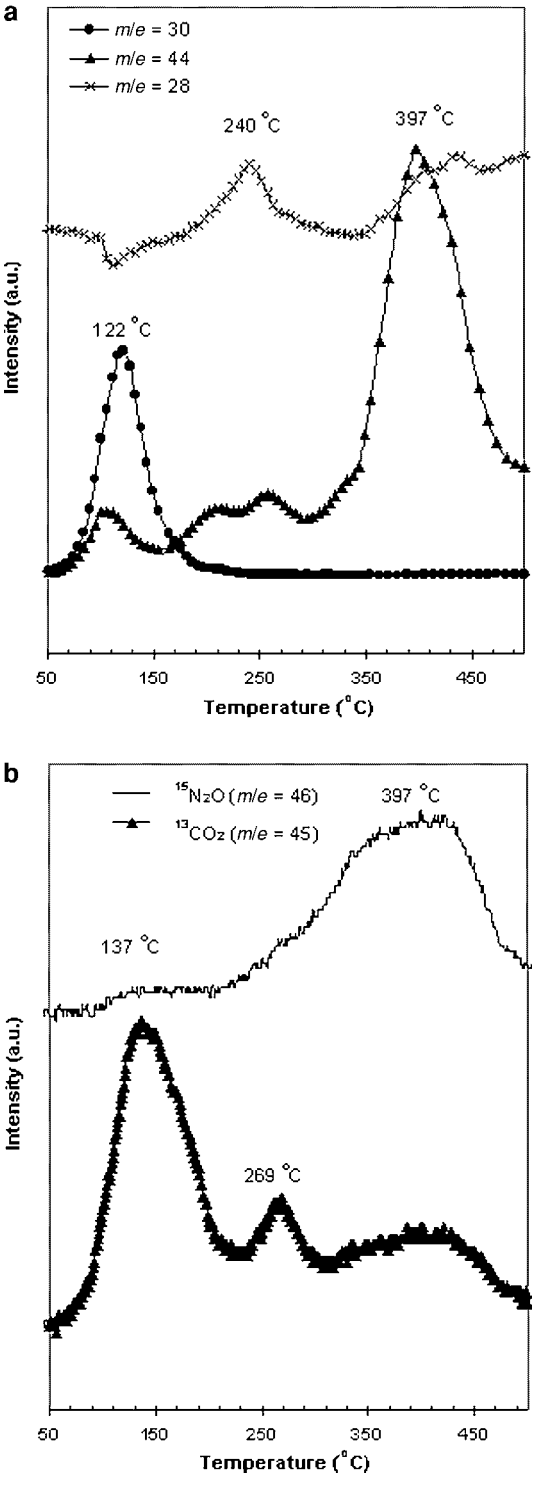

FIG. 6. TPD of (a) NO on CH_4-pre-adsorbed Gd–Pd/TiO_2 and (b) ^{15}NO on $^{13}CH_4$-pre-adsorbed Gd–Pd/TiO_2.

TPD Studies Using DRIFTS

DRIFTS-TPD of NO was performed over sol-gel TiO_2, Pd/TiO_2, and Gd–Pd/TiO_2 that were reduced in 33% H_2 in He. After *in situ* hydrogen reduction, the background spectra were taken under He at each temperature level. NO (5450 ppm in He) was adsorbed on the samples at 25°C for 30 min. The system was subsequently purged and heated under He and spectra were collected at different temperatures.

Figures 7a and 7b show a series of DRIFT spectra taken at 27, 113, 177, and 267°C under He after NO adsorption on the support. After exposure to NO for 30 min and flushing with He for 30 min, bands remained at 1618, 1600 (shoulder), 1581, 1524, 1442 (broad peak), 1369, 1352 (shoulder), 1288, and 1241 cm^{-1} at room temperature. In the higher-wavenumber region, a series of negative peaks at 3721 and 3671 cm^{-1} that are characteristics of surface hydroxyl groups were observed (Fig. 7b). This indicates that the surface hydroxyl were involved in reaction with NO to form certain nitrogen-oxo species. The bands at 1618–1650, 1442, and 1350–1400 cm^{-1} were thermally stable up to 177°C, but the bands at 1524 and 1288 cm^{-1} disappeared above 113°C. At the highest temperature, a pair of broad peaks at 1554 and 1442 cm^{-1} was visible which had a distinctive shape. The band at higher wavenumber is overlapped and difficult

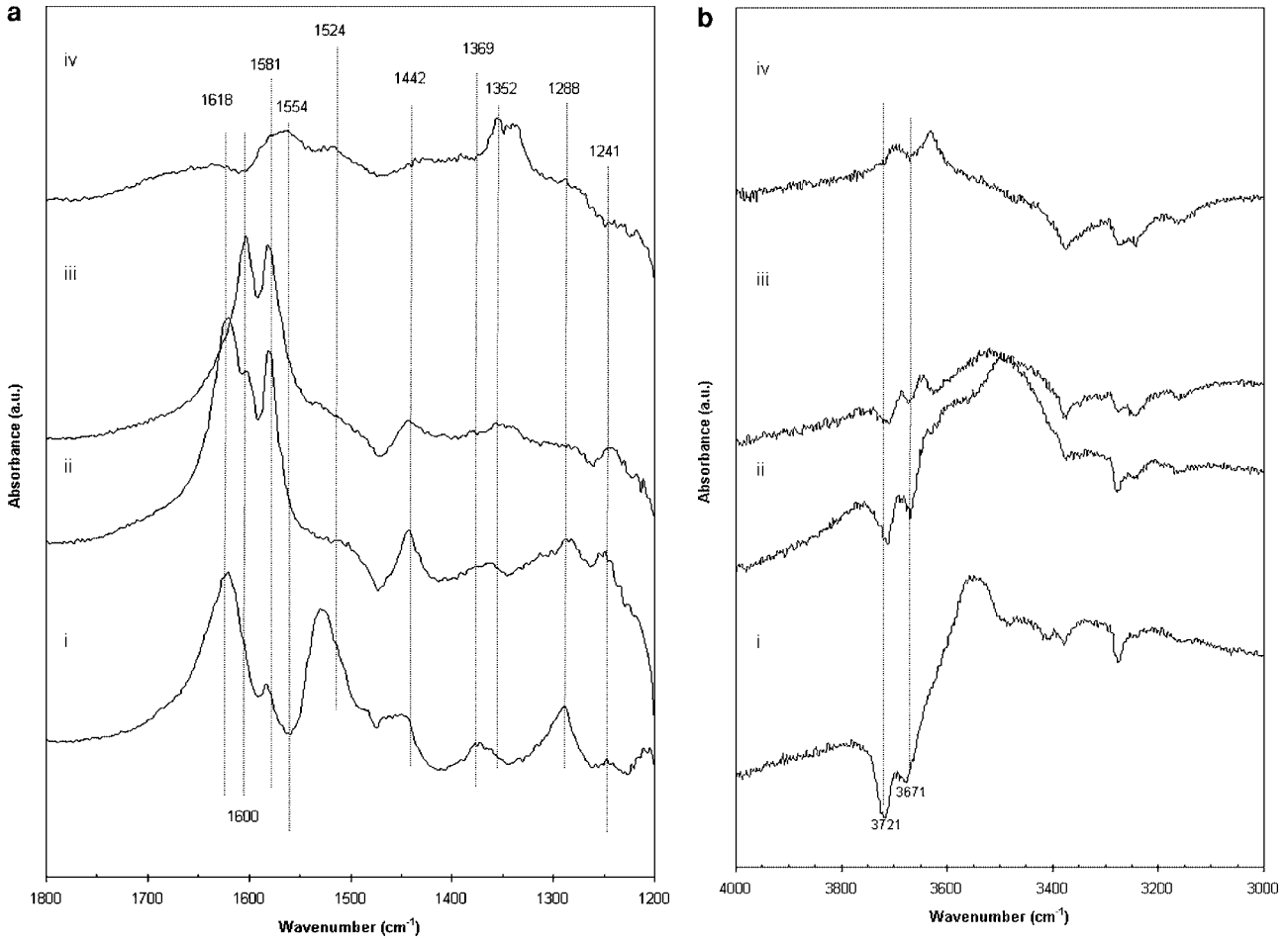

FIG. 7. DRIFT spectra of reduced TiO_2 after NO was adsorbed for 30 min and flushed in He for 30 min at i, 27°C; ii, 113°C; iii, 177°C; and iv, 267°C. (a) 1200–1800 cm^{-1} region, (b) 3000–4000 cm^{-1} region.

to distinguish from other nitrate species; however, due to the band split and the shape, they are likely to be different types of nitrogen-containing oxo species which arose from thermal transformation of other species.

The feature at 1618 cm^{-1} was attributed to bridging nitrate formed on oxide surfaces (32–36). The intensity of bands at 1600 and 1580 cm^{-1} with the associated band of 1241 cm^{-1} went through a maximum and were assigned as bidentate nitrate species (32, 34, 36). The features at 1524 and 1288 cm^{-1} that disappeared with increasing temperature were assigned to monodentate nitrate species because these species are reported to have vibrational frequencies at 1520–1480 cm^{-1} ($NO_{2,asy}$) and 1330–1250 cm^{-1} ($NO_{2,sym}$) (32–34, 37). Although much weaker in intensity, these bands seem to reappear at 267°C. The thermally stable features around 1352 cm^{-1} were assigned to nitro species (33, 34). Thermally transformed species at 1554 and 1442 cm^{-1} could be assigned as a nitro–nitrito complex (32). Hadjiivanov *et al.* investigated NO_2 adsorption on TiO_2 using FTIR spectroscopy (32). They showed that the adsorption of NO_2 on the titania surface led to formation of various nitrate species through participation of the H-bonded hydroxyl groups on anatase. When the sample was heated under vacuum after NO_2 exposure at room temperature, a nitro–nitrito complex was formed (32).

Figure 8 shows the DRIFT spectra at different temperature levels on reduced Pd/TiO_2 after NO exposure at room temperature. The bands at 1751, 1618, 1522, 1424, 1317, 1200 (shoulder), and 1162 cm^{-1} were observed at room temperature. The bands at 1162 and 1200 cm^{-1} and characteristic frequencies of NH_{3sy} coordinated to β and α Lewis and sites, respectively. Since prior to NO adsorption the catalyst was reduced in H_2/He mixture at 200°C, it is possible that chemisorbed hydrogen participated in reaction with adsorbed NO to form ammonia which is observed on Lewis acid sites. When comparing Figs. 7 and 8, it was found that the relative intensity ratio of monodentate nitrate species (1522 and 1317 cm^{-1}) to bridged nitrate species (1617 cm^{-1}) at room temperature was reversed on Pd/TiO_2 compared to TiO_2. On Pd/TiO_2, the intensity of the bands for monodentate at 1522/1317 cm^{-1} and coordinated NH_3 at 1162/1200 cm^{-1} decreased

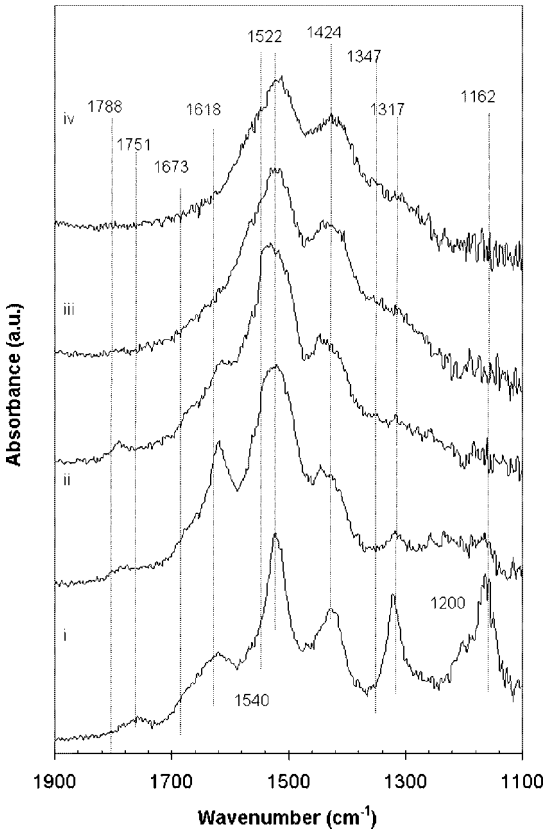

FIG. 8. DRIFT spectra of reduced Pd/TiO_2 after NO was adsorbed for 30 min and flushed in He for 30 min at i, 27°C; ii, 113°C; iii, 194°C; and iv, 329°C.

simultaneously and completely disappeared at 194°C. At this temperature, the bands that appear around the 1530–1550 cm^{-1} region are assigned to nitro–nitrito species as opposed to monodentates, since the lower temperature feature of the 1522/1317 cm^{-1} pair is no longer there. The band for bridged nitrate at 1618 cm^{-1} grew stronger at 113°C as monodentate and ammonia species disappeared. This seems to suggest that NH_3 may be involved in transforming Ti–ONO_2 to Ti–O_2NO. Hadjiivanov *et al.* introduced NH_3 to adsorbed NO_2 on anatase surface and saw the transformation of bridged/bidentate nitrate to monodentate (32). They proposed that protonation of ammonia by water molecules is involved in the transformation. Our observation suggests that a reverse scheme may also be possible for monodentate nitrate transformation to bridged nitrates.

There was a small band at 1751 cm^{-1} which appeared at room temperature and which was absent on the bare TiO_2 support. This species disappeared at 113°C; however, there was a small band that formed at 1788 cm^{-1} above 113°C, which disappeared at 329°C. This region is characteristic of NO species linearly adsorbed on Pd sites (38–41).

Figure 9 presents the DRIFT spectra taken on reduced Gd–Pd/TiO_2 under the same conditions as shown in Fig. 8. The types of bands observed in the presence and absence of Gd were very similar to each other. However, one major difference is that the band in the 1740–1790 cm^{-1} region is very prominent over the Gd–Pd/TiO_2.

There are many reports in the literature that refer to linear NO adsorption on metallic Pd giving rise to a band around 1750 cm^{-1} (38, 40–45). The effect of pre-adsorbed oxygen on Pd has been shown to shift the band frequency of linear NO to higher wavenumber (41) due to electronegativity of oxygen reducing the electron density at Pd, which results in weakening of the back-bonding to NO (41). The band that appears between 1775 and 1795 cm^{-1} has been assigned to Pd^+–NO, the linear NO adsorbed on partially oxidized Pd sites which has an average oxidation state of 1+ (45) and has been differentiated from the band in the 1740–1750 cm^{-1} region, which is attributed to Pd^0–NO. The crystal plane of Pd (e.g., (100) vs (111)) on which NO adsorbs, the surface temperature, and the surface coverage (due to dipole coupling effect) are also reported to shift the band position in this region (40–42, 44). Another species that can account for the spectral features around 1740–1755 cm^{-1} is N_2O_4 adsorbed on TiO_2 or on Pd sites (24, 35).

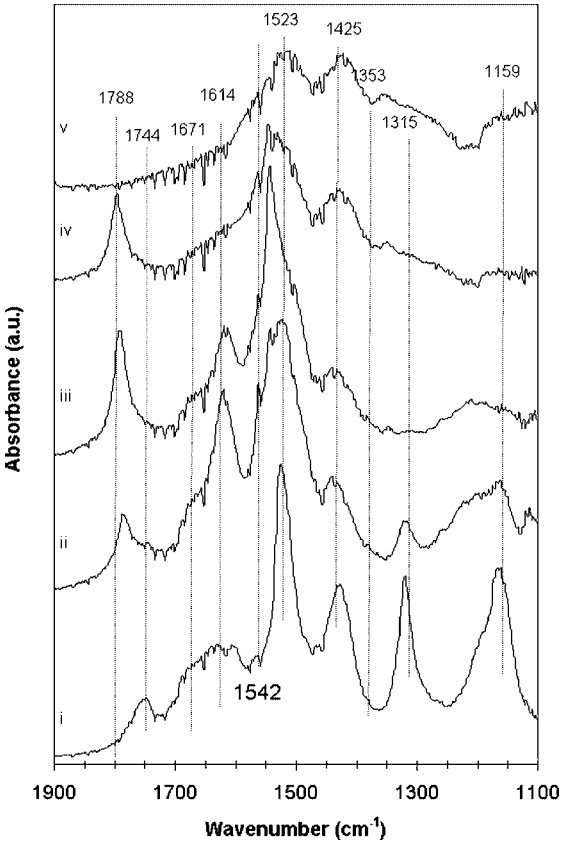

FIG. 9. DRIFT spectra of reduced Gd–Pd/TiO_2 after NO was adsorbed for 30 min and flushed in He for 30 min at i, 27°C; ii, 113°C; iii, 194°C; and iv, 329°C.

Regardless of the oxidation state of Pd, the presence of Gd seems to enhance the rate of NO adsorption or readsorption onto Pd sites relative to the Gd-free catalyst. The intensity of the linearly adsorbed NO band was seen to increase at higher temperatures under He flow along with the changes observed in the nitrate region of the spectra. It is plausible that, at higher temperatures, transformation/decomposition of other nitrogen-oxo species contribute to the surface concentration of linearly adsorbed NO.

DRIFTS-TPD after simultaneous adsorption of NO and CH_4 at room temperature over reduced Gd–Pd/TiO_2 is shown in Figure 10. After the catalyst surface was reduced in 33% H_2/He mixture, it was exposed to a mixture of 0.46% NO and 0.89% CH_4 for 30 minutes at 25°C. Subsequently, vacuum was pulled in the environmental chamber to eliminate the gas phase. Under flow of NO + CH_4 at 25°C, bands were observed at 1752, 1622, 1574, 1495, 1431, 1364, 1301, 1200 (shoulder), and 1172 cm^{-1} (Fig. 10a). Bridged nitrate at 1622 cm^{-1} was the most prominent band under flow conditions. The presence of coordinated $NH_{3,sym}$ on Lewis acid sites is seen at 1172 and 1200 cm^{-1}. There was a band at 1495 cm^{-1}, which characterizes $NH^{+}_{4,asy}$ and it indicates the presence of Brønsted acid sites on the surface. The asymmetric and symmetric deformations of CH_3 have vibrational frequencies around 1450 and 1350 cm^{-1}, respectively (46, 47). Although nitro species do appear in the same region, the weak signal (~1431/1364 cm^{-1}) in this region could be related to CH_x species. When the system was evacuated, the bands for monodentate nitrate (around 1530/1319 cm^{-1}) became more prominent, accompanied by a decrease in the bridged nitrate signal, which could also suggest the transformation of bridged/bidentate nitrates to monodentate nitrates as proposed in the literature for anatase titania: Ti–$O_2NO + H_2O + NH_3 \rightarrow Ti(OH^-)(ONO_2) + NH^{4+}$ (32).

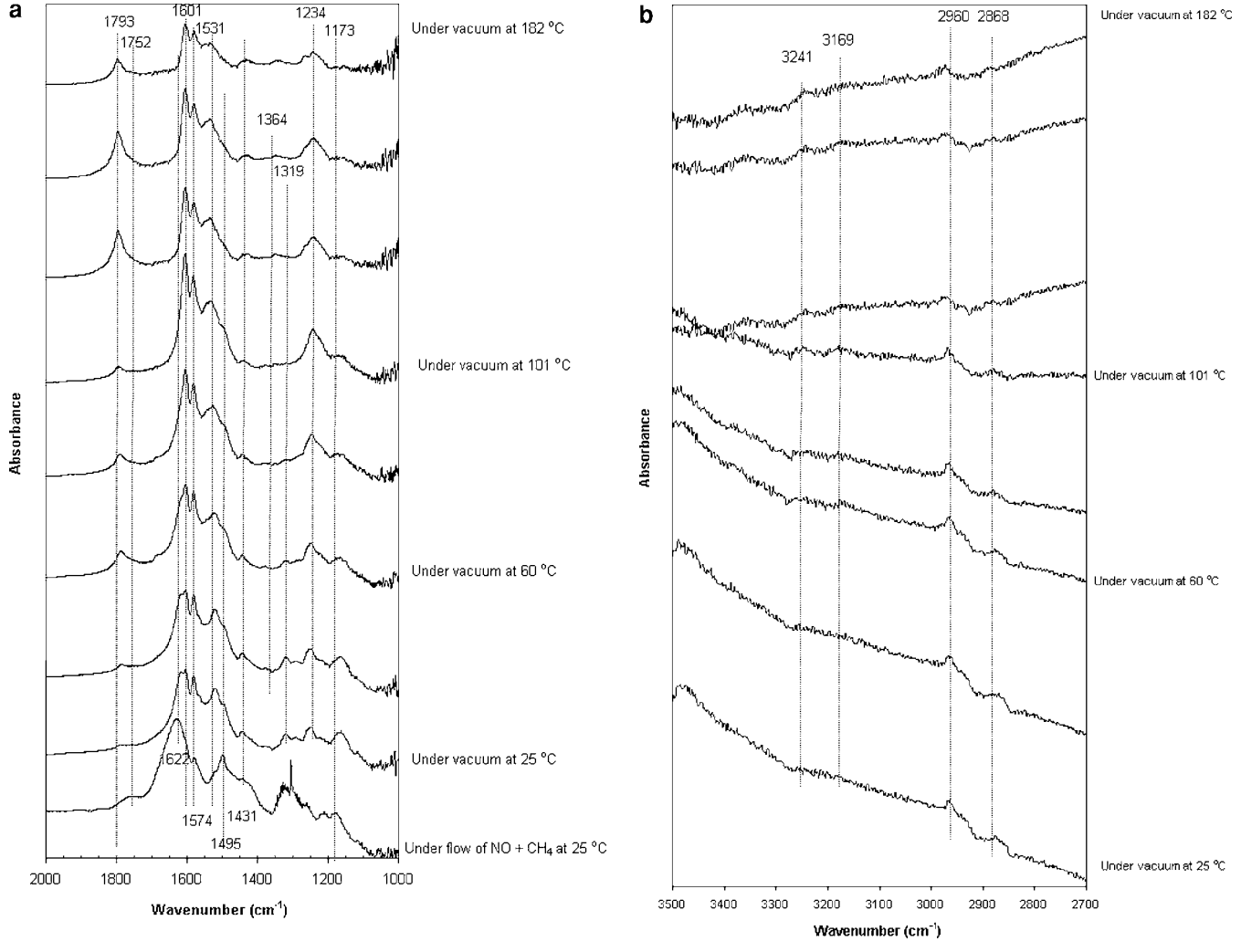

FIG. 10. DRIFT spectra under vacuum of reduced Gd–Pd/TiO_2 after NO + CH_4 (0.46% NO and 0.89% CH_4) adsorption for 30 min at room temperature: (a) 1000–2000 cm^{-1} region, (b) 2700–4000 cm^{-1} region.

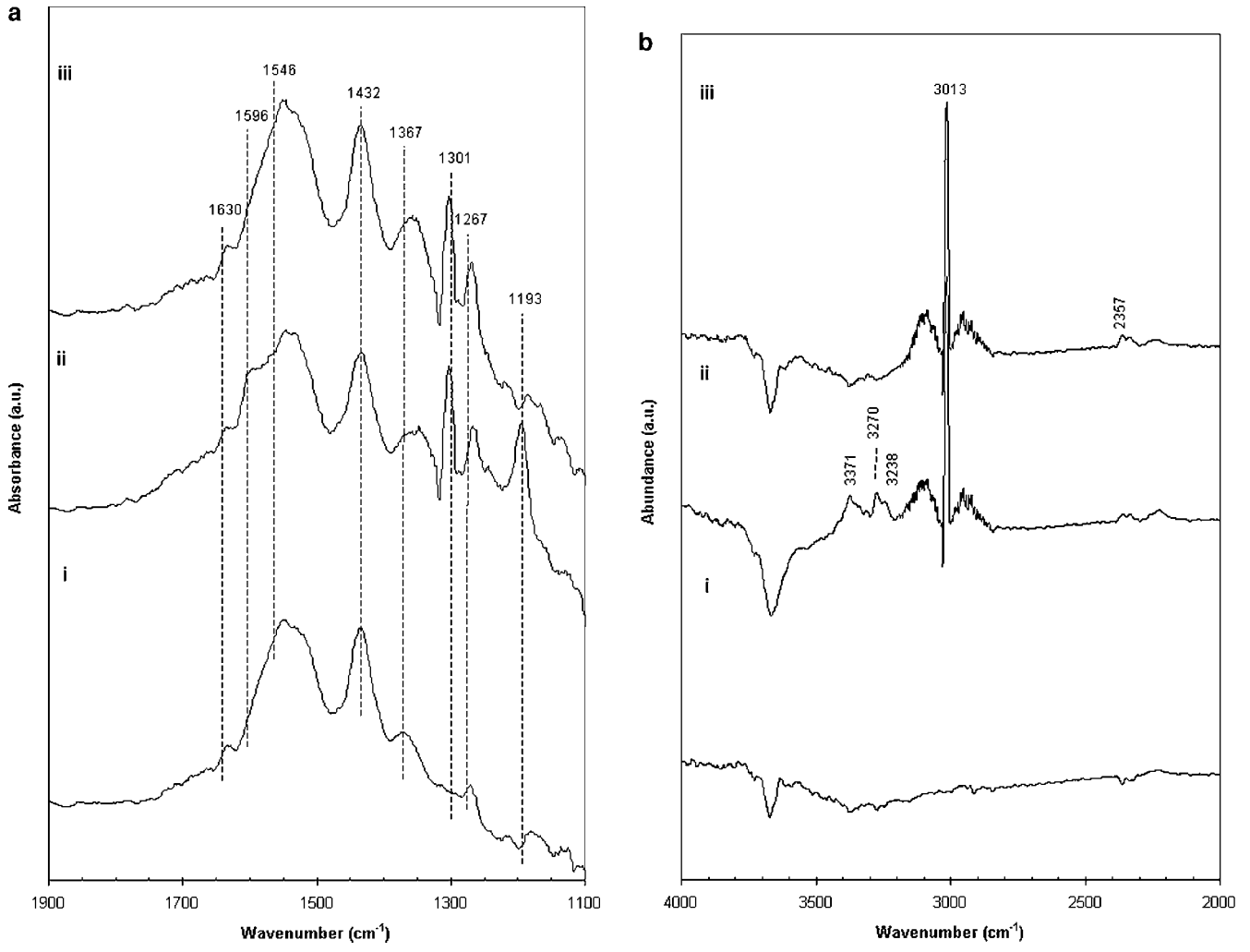

FIG. 11. DRIFT spectra under NO → NO + CH_4 → NO + CH_4 + O_2 flow at 300°C on reduced TiO_2: i, 1780 ppm NO; ii, 1780 ppm NO, 2.13% CH_4; iii, 1780 ppm NO, 2.13% CH_4, 3000 ppm O_2. (a) 1100–1900 cm^{-1} region, (b) 2000–4000 cm^{-1} region.

As the temperature is increased under vacuum, the band for linear NO on Pd at 1752 cm^{-1} gradually shifts to higher wavenumber (1793 cm^{-1}) and grows in intensity, exhibiting a similar behavior to that observed in Fig. 9. The shift to higher wavenumbers, which accompanies the increase in intensity is likely due to dipole–dipole coupling effect, because higher intensity would imply higher surface coverage.

Figure 10b shows evidence for the presence of adsorbed CH_x species through the characteristic IR bands for –CH and $–CH_2$ stretching at 2960 and 2868 cm^{-1}. Also, the bands in the 3410–3180 cm^{-1} region that corresponds to N–H stretching for adsorbed NH_3 on Lewis acid sites are observed above 120°C.

DRIFT Spectra under Flow (NO → NO + CH_4 → NO + CH_4 + O_2)

DRIFT spectra were taken over reduced sol-gel TiO_2, Pd/TiO_2, and $Gd–Pd/TiO_2$ under flow of NO, NO + CH_4, and NO + CH_4 + O_2 sequentially (NO = 1780 ppm, CH_4 = 2.13%, O_2 = 2900 ppm). Spectra were taken after the catalyst was exposed to the gas mixture for 30 min at 300°C. The spectrum taken under the flow of NO over the reduced TiO_2 (Figs. 11a and 11b) was quite comparable to the spectrum in Fig. 7 (curve ii), which was taken at the same temperature under He after NO exposure at room temperature. The distinct features for nitro–nitrito complex (1546/1432 cm^{-1}), low intensity monodentate nitrate (1546 (overlapped)/1267 cm^{-1}), nitro species (1367 cm^{-1}), and low-intensity bridged nitrate (1630 cm^{-1}) were observed. When CH_4 was added to the NO flow, the bands at 1191 cm^{-1} and multiplex at 3400–3250 cm^{-1} were observed, suggesting the formation of molecular NH_3 on Lewis acid sites. Gas-phase CH_4 is observed at 3013 and 1301 cm^{-1}. Surface species seemed to be unaffected with the incorporation of CH_4 into the gas phase, indicating that anatase titania alone is not active for reduction of NO. When O_2 is introduced to the NO + CH_4 flow, the bands associated

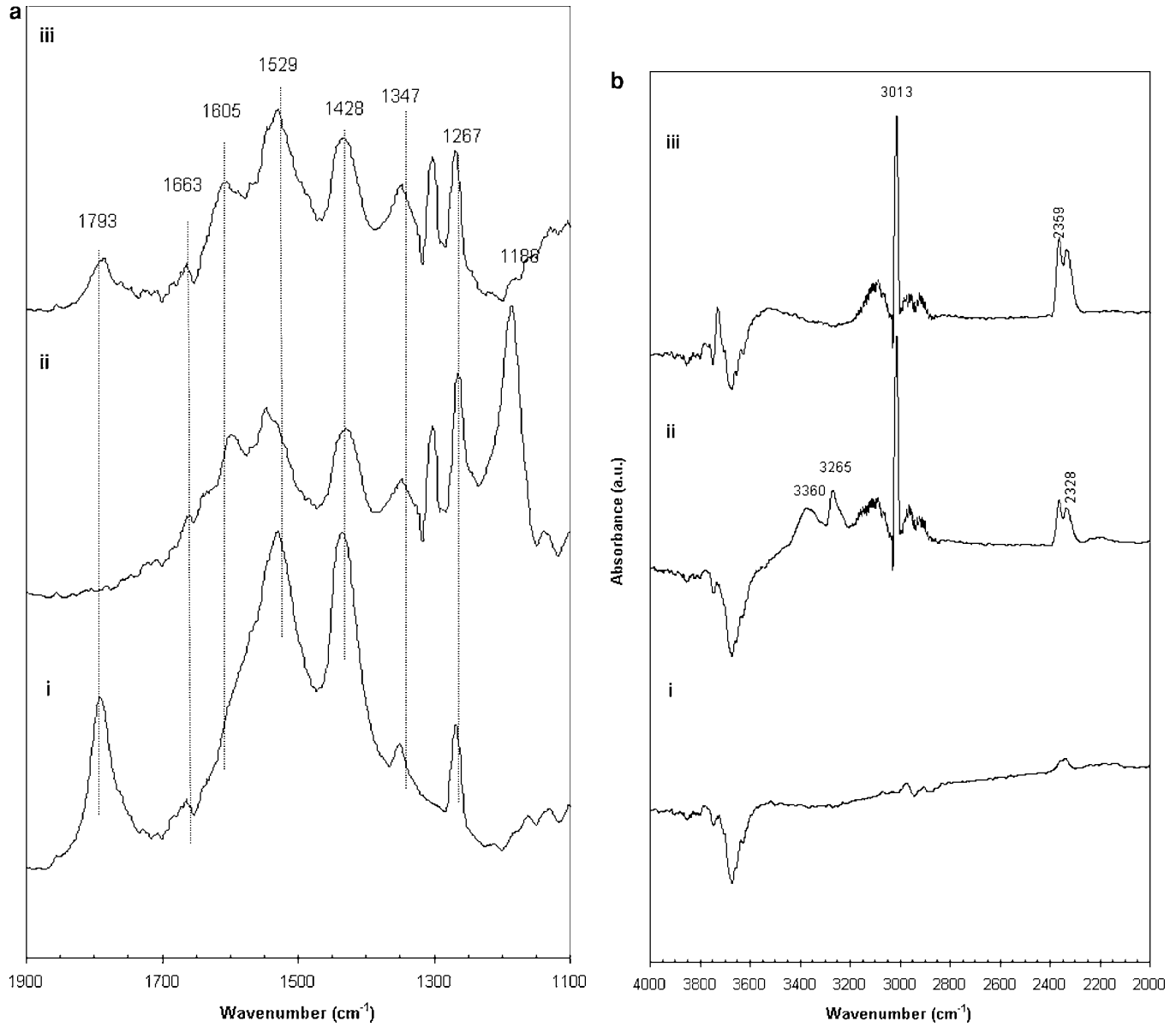

FIG. 12. DRIFT spectra under NO → NO + CH_4 → NO + CH_4 + O_2 flow at 300°C on reduced 2% Pd/TiO_2: i, 1780 ppm NO; ii, 1780 ppm NO, 2.13% CH_4; iii, 1780 ppm NO, 2.13% CH_4, 3000 ppm O_2. (a) 1100–1900 cm^{-1} region, (b) 2000–4000 cm^{-1} region.

with NH_x disappeared, indicating that this species is highly reactive toward O_2. There were no other changes in the spectra when O_2 was introduced to the gas phase.

The same experiment was performed on reduced Pd/TiO_2 as shown in Fig. 12. Under NO flow, the band at 1793 cm^{-1}, corresponding to NO species linearly adsorbed on Pd, was observed in addition to what was observed on TiO_2 shown in Fig. 11. The relative intensity of the bands in 1400–1600 cm^{-1} is still quite high, indicating that monodentate nitrate or nitro–nitrito complex species continue to have a substantial presence over the Pd/TiO_2 at 300°C. Under NO + CH_4 flow in Fig. 12a (curve ii), we see the disappearance of the Pd–NO species coupled with the appearance of a very intense band at 1186 cm^{-1}, signaling the formation of NH_3. The relative intensity of 1186 to 1529 cm^{-1} was much higher over the Pd/TiO_2 compared to the bare support (Fig. 11a, curve ii). It should be noted that Fig. 12, curve ii represents the active condition where complete NO conversion is obtained. Also in the same figure, a drastic decrease in the intensity of the 1529 and 1428 cm^{-1} bands was observed in the presence of CH_4. When O_2 was introduced to the NO + CH_4 flow shown in Fig. 12a (curve iii), NH_x species disappeared while at the bands 1529 and 1428 cm^{-1} species remained the same on the surface.

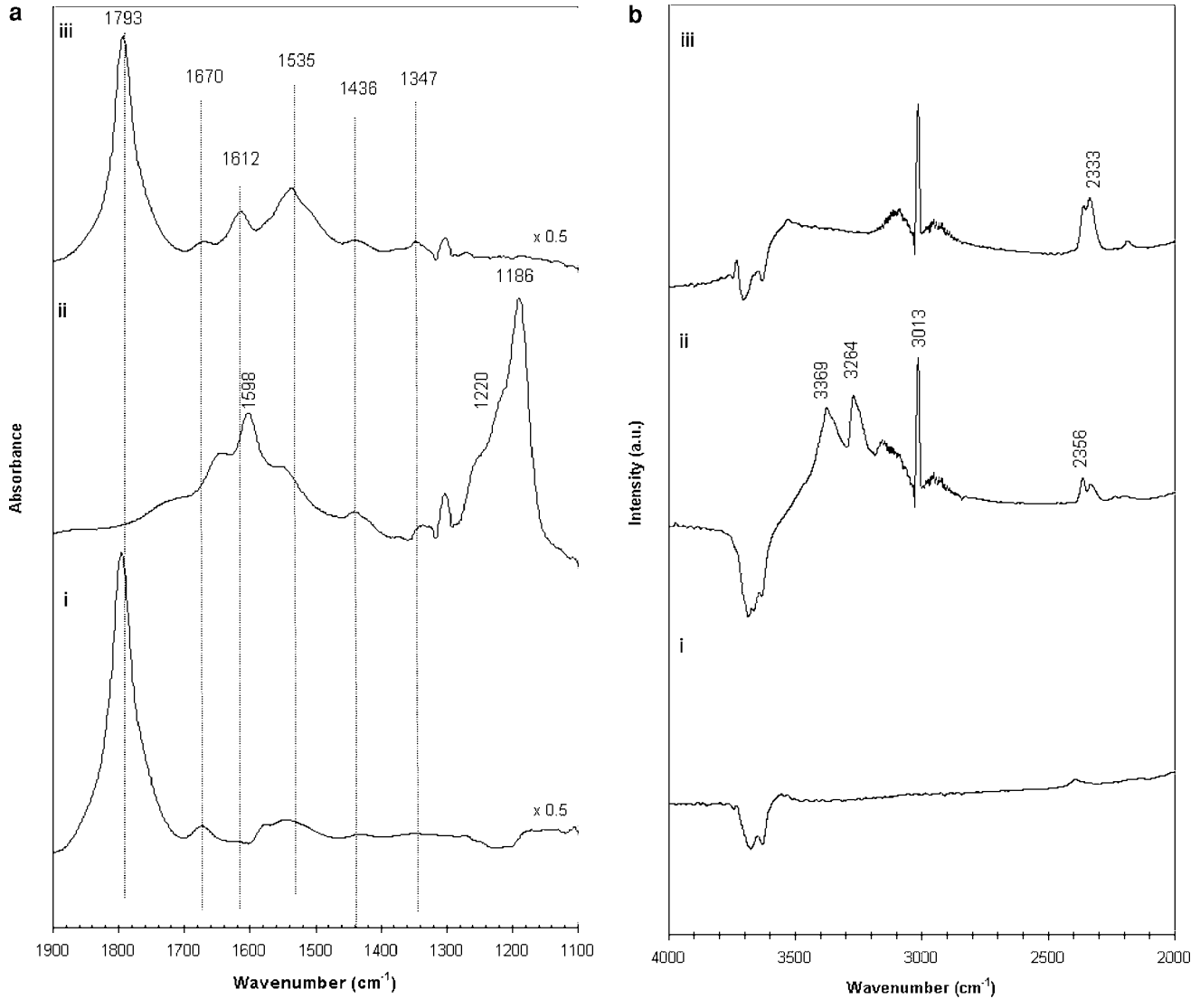

FIG. 13. DRIFT spectra under NO → NO + CH_4 → NO + CH_4 + O_2 at 300°C on reduced 1% Gd–2% Pd/TiO_2: i, 1780 ppm NO; ii, 1780 ppm NO, 2.13% CH_4; iii, 1780 ppm NO, 2.13% CH_4, 3000 ppm O_2. (a) 1100–1900 cm^{-1} region, (b) 2000–4000 cm^{-1} region.

Concurrently, the Pd–NO band, although much weaker in intensity, reappeared.

Over the reduced Gd–Pd catalyst (Fig. 13a), the band at 1793 cm^{-1} (linear NO on Pd) was by far the most dominant feature at 300°C under NO flow. The intensity of monodentate nitrate and nitro species relative to the Pd–NO peak was much lower on this catalyst compared to the Gd-free catalyst. The presence of Gd clearly seemed to enhance the adsorption of NO as linear Pd–NO species. This could be due to a better coverage (better Pd dispersion) of the TiO_2 surface, which is seen to lead to the formation of nitrates. The behavior under NO + CH_4 flow was similar to that observed over the Pd/TiO_2 catalyst under the same conditions. The Pd–NO feature disappeared while a strong band at 1186 cm^{-1}, accompanied by the appearance of N–H stretching characterized by the multiplex at 3400–3250 cm^{-1}, appeared. Also visible in the spectrum was the band at 1598 cm^{-1}, which is associated with $NH_{3,asy}$. Features associated with NH_3 disappeared and the Pd–NO band reappeared when O_2 was introduced to the flow.

Figures 14a and 14b show the spectra taken over the oxidized Gd–Pd/TiO_2. Under NO flow, the relative intensity of linear Pd–NO to nitrate species on the support was decreased over the oxidized sample. Moriki *et al.* and Hoost *et al.* observed similar results on oxidized Pd/SiO_2 and Pd/Al_2O_3 catalysts, respectively. When NO was adsorbed on the oxidized catalyst, the peak intensity of linearly adsorbed NO decreased drastically compared to the reduced catalyst (38), suggesting that oxidation of Pd to PdO might result in steric hindrances of the NO adsorption sites on Pd.

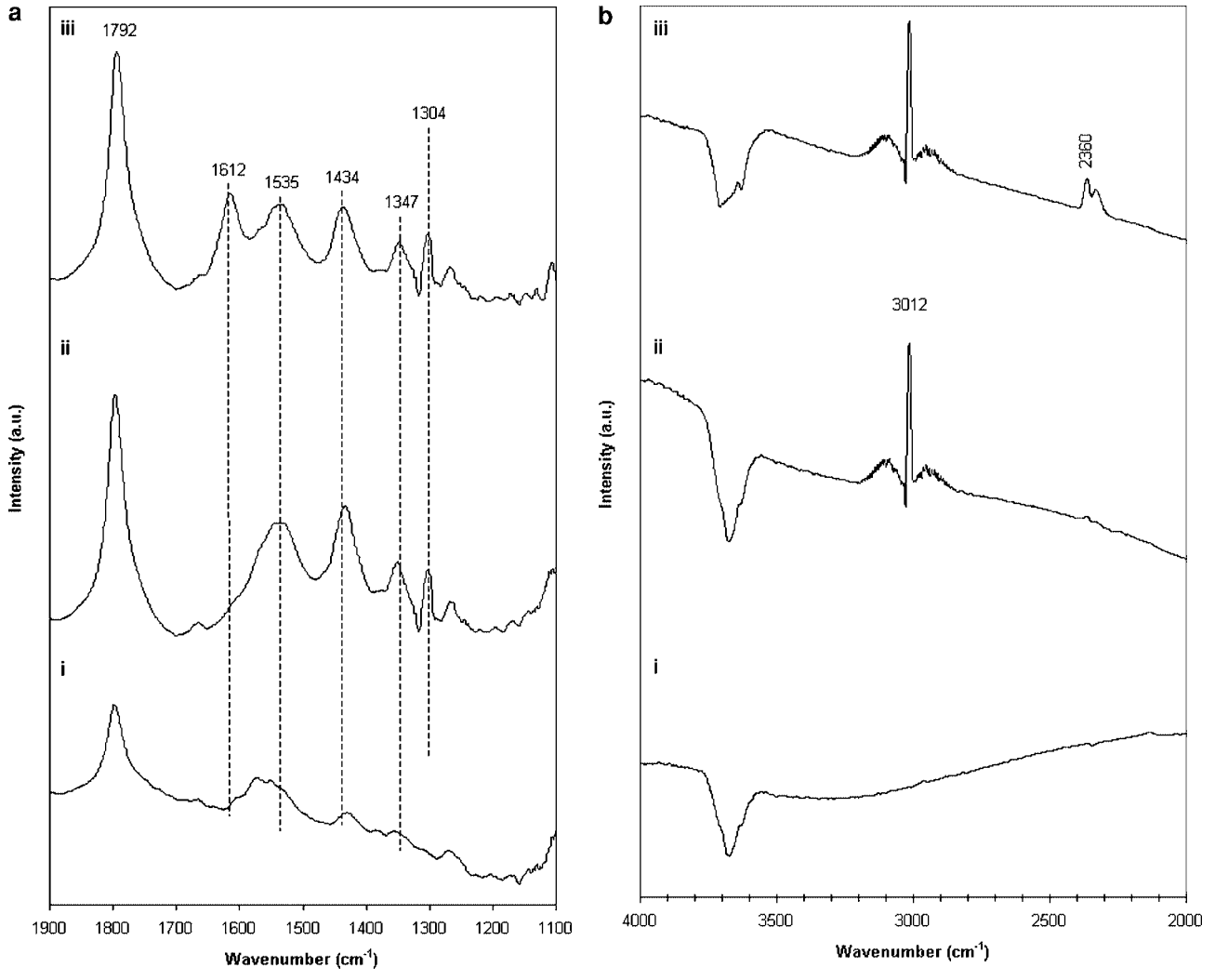

FIG. 14. DRIFT spectra of NO → NO + CH_4 → NO + CH_4 + O_2 adsorption at 300°C on oxidized Gd–Pd/TiO_2: i, 1780 ppm NO; ii, 1780 ppm NO, 2.13% CH_4; iii, 1780 ppm NO, 2.13% CH_4, 3000 ppm O_2. (a) 1100–1900 cm^{-1} region, (b) 3000–4000 cm^{-1} region.

When CH_4 was introduced to NO flow, there was no formation of NH_x species. The relative intensity of the Pd–NO band increased, contrary to what was observed over the reduced catalyst.

In order to further probe the intermediate surface species during NO + CH_4 reaction (100% NO conversion condition), the surface was rapidly cooled to room temperature under He subsequent to exposing the catalyst to NO + CH_4 flow at 300°C for 30 min. The spectra obtained over Gd–Pd/TiO_2 during NO + CH_4 reaction at 300°C and after quenching to room temperature are presented in Figs. 15a and 15b, respectively. The main species on the surface are the NH_x with a band at 1185 cm^{-1} ($NH_{3,sym}$) and a corresponding band at 1598 cm^{-1} ($NH_{3,asy}$). When the surface was quenched, sharp peaks at 1743 and 1677 cm^{-1} emerged. The appearance of 1743 cm^{-1} under highly reducing conditions seems to indicate that this band is likely to be due to linear NO on metallic Pd sites. However, the possibility of N_2O_4 contributing to these spectral features cannot be excluded. The peak at 1677 cm^{-1} was attributed to bent NO on Pd (40). There is a small shoulder at 1772 cm^{-1}, which could indicate the presence of linear NO on partially oxidized Pd. Figure 16 shows the spectra taken over reduced Gd–Pd/TiO_2 under the flow of NO + CH_4 + O_2 (curve a) and after quenching (curve b). Again, under these conditions, the catalyst shows partial deactivation. Under NO + CH_4 + O_2 flow in Fig. 16 (curve a), Pd^+–NO species at 1792 cm^{-1} were found to be dominant, with 1663 cm^{-1} (bent Pd–NO) also present as a weaker band. After quenching, the 1792 cm^{-1} band became even more dominant, supporting our assertion that this is indeed Pd^+–NO species. There was a small shoulder at 1743 cm^{-1} signaling the presence of Pd^0–NO species still left on the surface. This spectrum (Fig. 16, curve b) is pronouncedly different from the one presented in

Fig. 15 (curve b), which was obtained following an oxygen-free reaction. The reversal of the relative intensities of the 1743 to 1792 cm^{-1} bands when oxygen was used in the feed seems to give additional support to the assignment that the latter band is due to Pd^{+}–NO. The fact that the 1772 cm^{-1} band (Fig. 15, curve b) shifted to 1792 cm^{-1} (Fig. 16, curve b) after the catalyst was exposed to oxygen in the feed could be due to this electronic effect. It is also conceivable, however, that the shift is due to a higher NO coverage caused by a lower conversion of NO in the presence of oxygen.

In order to examine the role of NH_x in the reduction of the Pd–NO species, 1780 ppm NO in He was flowed over reduced Gd–Pd/TiO_2 at 300°C for 30 min followed by addition of 3000 ppm NH_3 to the NO–He stream. Spectra taken under NO flow before NH_3 introduction is shown in Fig. 17 (curve a). Figure 17 (curves b and c) represents spectra taken 20 and 30 min after NH_3 introduction, respectively. In Fig. 17 (curve b), taken 20 min after NH_3 exposure, the 1794 cm^{-1} band was completely gone and those bands

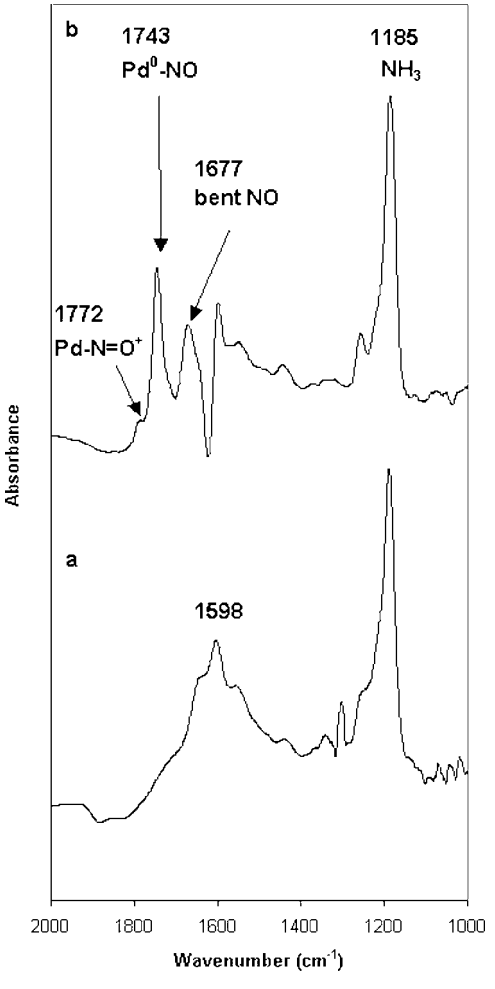

FIG. 15. DRIFT spectra of reduced Gd–Pd/TiO_2 (a) under NO + CH_4 flow (1780 ppm NO, 2.13% CH_4) at 300°C and (b) under He at room temperature after quenching.

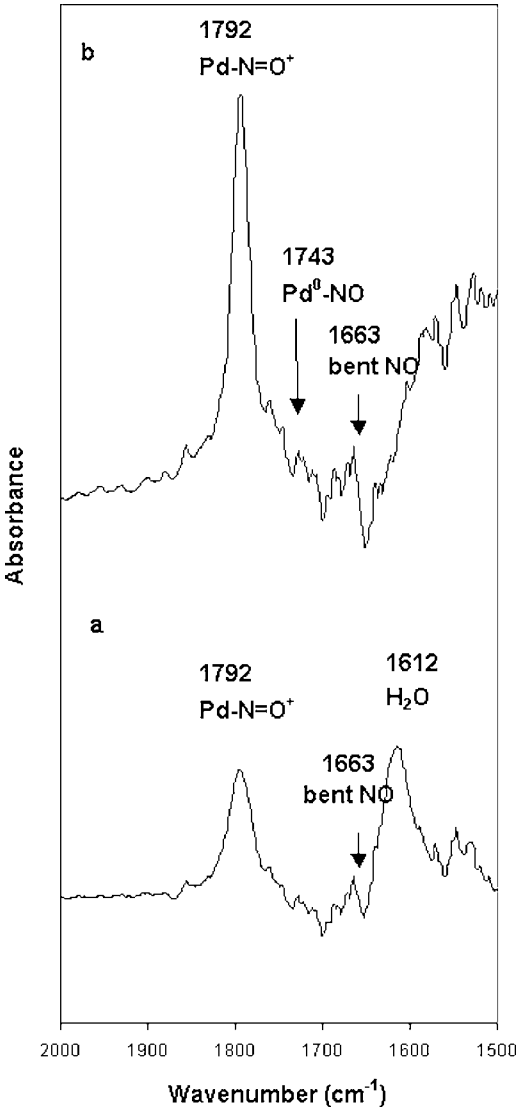

FIG. 16. DRIFT spectra of reduced Gd–Pd/TiO_2 (a) under NO + CH_4 + O_2 flow (1780 ppm NO, 2.13% CH_4, 2900 ppm O_2) at 300°C and (b) under He at room temperature after quenching.

corresponding to NH_3 appeared. We also observed N_2O in the gas phase as indicated by a pair of bands at 2231 and 2188 cm^{-1}.

DISCUSSION

The DRIFT study showed that formation of bridged, bidentate, and monodentate nitrate species after NO adsorption was possible on TiO_2 support and on Pd-based catalysts supported on TiO_2. Ramis *et al.*, who observed the formation of nitrates following NO adsorption on TiO_2, suggested that NO could be first oxidized to NO_2 at Ti^{4+} sites and further oxidized to NO_3^- (48). The Ti^{4+} sites are most likely located on the edges where ions with a high number of coordination vacancies are found (48).

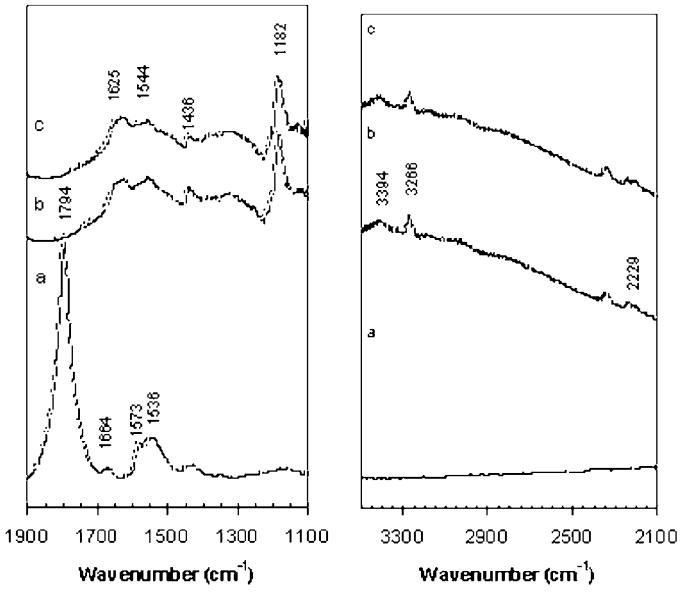

FIG. 17. DRIFT spectra of NO → NO + NH_3 adsorption at 300°C on reduced Gd–Pd/TiO_2: (a) 1780 ppm NO; (b) 20 min in 1780 ppm NO, 3000 ppm NH_3; (c) 30 min.

Hadjiivanov *et al.* (32) studied NO_2 adsorption on TiO_2 and suggested that bidentate and monodentate nitrate could be formed through the interaction of NO_2 with hydrogen-bound hydroxyl groups. Our DRIFT spectra also indicated that free hydroxyl groups were involved in the formation of nitrate species on the titania surface. We observed the presence of a broad band at 3500 cm^{-1} that is characteristic of O–H stretching of hydrogen bound hydroxyl groups where its proton is weakly bonded to another oxygen atom. It is plausible that nitrate formation proceeds initially by NO oxidation to NO_2 on Ti^{4+} sites, after which NO_2 is converted to nitrate through an interaction with hydroxyl groups.

Thermal transformation of some of bridged/bidentate and monodentate nitrate into more stable compounds such as nitro, nitrito, and linear NO was observed over the Pd and Gd–Pd catalysts with increasing temperature. As part of transformation of nitrate species, linear Pd–NO was also formed at higher temperatures under He flow. The thermal transformation of nitrate species could also be linked to the desorption of NO, N_2, and N_2O from the Gd–Pd catalyst surface through decomposition/coupling at temperatures 127°C (LT), 182°C (MT), and 275°C (HT) (Fig. 3). NO desorption from the LT site is most likely due to monodentate nitrate species, which were shown to disappear from the surface at relatively low temperatures in the *in situ* DRIFTS-TPD experiments. The same experiments seemed to suggest that NO desorption at the midtemperature range is a result of decomposition of the bridged nitrates. In the high-temperature range, on the other hand, desorption of NO is likely to result from linear NO on Pd sites. The NO-TPD experiments have shown N_2 and N_2O desorbing at the same temperature with the high-temperature NO desorption features. The fact that the desorption temperatures of N_2 and N_2O are the same suggests that the formation of these two species involve the same type of sites and/or the same rate-determining step. Similar observations have been reported by Sharpe *et al.*, who investigated the relative selectivity of N_2 and N_2O production from NO adsorption on Pd(110) as a function of coverage and surface temperature using a molecular beam. They calculated activation energies for various steps in the mechanism where adsorbed NO dissociates to $N_{(a)}$ and $O_{(a)}$ followed by coupling of two $N_{(a)}$ to form N_2 ($2N_{(a)} \rightarrow N_{2(g)}$). A competing reaction with this would be ($N_{(a)} + NO_{(a)} \rightarrow N_2O_{(a)}$), followed by desorption of N_2O into the gas phase. It is also possible for adatoms of oxygen to couple and desorb as molecular oxygen or to diffuse to the bulk. The dissociation of NO appears to be the rate-determining step common to the formation of both N_2 and N_2O. The relative selectivity of these two species is a function of surface temperature, the surface coverage, and the extent of surface oxidation (28).

The absence of the HT-NO desorption feature on Pd/TiO_2 (Fig. 3, curve b) and the much lower intensity of the linear NO band (Fig. 8) observed in the DRIFT spectrum provides additional support that the HT-NO desorption feature indeed originates from the Pd–NO sites. Also, this was noted as the major difference between the Pd and Gd–Pd catalysts in surface species formation following NO adsorption (Figs. 8 and 9).

One possible explanation for the difference observed in abundance of the linearly adsorbed NO species between Pd and Gd–Pd catalysts could be that the incorporation of Gd into the catalyst matrix increases the number and/or accessibility of the Pd sites. When Pd metal is more uniformly dispersed on the surface, there are more Pd sites available for linear NO formation through the thermal transformation or decomposition of nitrate species. There is evidence in the literature that the dispersion of Pd increases with La, which plays a geometric role in disrupting the agglomeration of Pd^0 (49). In our studies where other lanthanide elements (Ce, Yb, La) were used as dopants for Pd/TiO_2 catalysts in NO–CH_4 reaction, we observed a similar effect in the catalytic behavior (18). It is highly likely that this effect is not specific to Gd, and other rare-earth elements can serve the same function. There have also been reports in the literature about the effect of lanthanide elements on the particle size of titania crystals (50). The fact that, in our study, the surface area increased substantially with incorporation of Gd as well as other lanthanides also seems to agree with the suggestion that the role of Gd could be in controlling the crystal growth of TiO_2.

While the dispersion and crystal-size effect of Gd is likely to be an important factor in the catalytic performance of Pd/TiO_2 catalysts, an even more significant role for a Gd promoter may be related to its high electropositivity. Gd, which is much more electropositive than Pd, could act as

an oxygen scavenger keeping Pd atoms from oxidizing, and could affect the adsorption and reduction behavior of NO on Pd. Our steady-state reaction studies showed that metallic state of Pd was essential for NO reduction and the presence of Gd could substantially improve the oxygen tolerance of the catalyst by stabilizing Pd in the zero oxidation state (18). These conclusions were further substantiated by our postreaction XPS experiments and self-induced oscillation studies (15, 18). The *in situ* DRIFTS experiments performed following NO adsorption also point to changes in the nature of the Pd–NO species by the incorporation of Gd. We have observed differences in both the intensity and the position of the Pd–NO bands in Gd–Pd catalyst compared to the Gd-free catalysts. While the Gd-free catalysts showed very weak features in the region that corresponds to the vibrational frequency of linearly adsorbed NO, this band became much more intense with the addition of Gd. One needs to exercise caution, however, when comparing absolute band intensities over different catalysts since the particle-size differences could strongly affect the IR band intensities. Therefore, it may be more appropriate to compare relative intensities of the bands. Another difference observed was the shift of the Pd–NO band to lower frequencies over the Gd–Pd catalysts. There have been reports in the literature that refer to the shifts in the Pd–NO band position as a function of surface oxygen concentration (40, 41). Grill *et al.* have studied the effect of oxygen on NO adsorption over Pd/SiO_2. On the reduced catalyst, they observed the formation of linear NO on Pd at 1735 cm^{-1}. On the oxidized catalyst, this band shifted to higher wavenumbers. This shift arose because electronegative oxygen atoms reduced the electron density at Pd atoms, making fewer electrons available for back-bonding (41). Hoost *et al.* assigned the bands at 1753–1750 cm^{-1} to linearly adsorbed NO on reduced form of the Pd/Al_2O_3 catalysts and reported a higher likelihood for the formation of two-fold and triple-fold bridged species, possibly involving the support sites, over the oxidized catalysts (38).

Almusaiteer and Chuang assigned the bands at 1754 cm^{-1} and 1650 cm^{-1} to linear NO adsorbed on metallic Pd sites (Pd^0–NO) and to bent NO on Pd (Pd^-–NO), respectively. They attributed the bands at 1798 cm^{-1} to linear NO adsorbed on Pd^+ sites (Pd^+–NO) (45). When the catalyst was exposed to NO flow for a prolonged time, the only linear NO observed was Pd^+–NO, which indicated that metallic Pd could be oxidized to Pd^+ by the adsorbed oxygen (45). When pulses of CO were introduced to the NO–He stream flowed over the catalyst, the Pd^+–NO band decreased in intensity and the Pd^0–NO band reappeared, indicating that CO reduced the partially oxidized palladium to the reduced state (45). It is not clear if the presence of CO could have reduced the dipole coupling effect for NO in their experiments, but it remains a possibility. In our DRIFTS experiment where the system was quenched after $NO + CH_4$ flow over $Gd–Pd/TiO_2$ (Fig. 15), the 1772 and 1743 cm^{-1} bands were observed; however, the relative intensity of the bands suggested that formation of the latter band was favored under highly reducing conditions. When spectra taken in the absence or in the presence of oxygen (Figs. 15 and 16, respectively) are compared, a shift in linear NO band from 1772 to 1792 cm^{-1} was observed. Also noted in this spectrum taken under oxygen was the much lower intensity of the 1743 cm^{-1} band relative to the 1792 cm^{-1} band. These results suggest that the band at 1743 cm^{-1} is most likely Pd^0–NO while the linear NO band at higher wavenumbers (1772 to 1792 cm^{-1}) shifts to higher frequencies by the changes in the electron density at Pd.

While other explanations exist in the literature for shifts in the band position of the Pd–NO species in terms of the crystal planes that the NO species are adsorbed on (42), in our case it is more difficult to relate these shifts to different crystal planes of Pd since palladium exists as highly dispersed surface species without any apparent long-range order. On the other hand, the shift due to dipole coupling effect at higher surface coverage cannot be ruled out. Dipole coupling is likely to be an important factor, especially in those spectra where the intensity of the Pd–NO band was accompanied by a blue shift in the NO frequency. However, the electronic effect due to the electropositivity of the Gd is also important. When room-temperature NO adsorption spectra over the Pd and Gd–Pd catalysts are compared, we see a more intense Pd–NO band at a lower wavenumber over the Gd–Pd catalysts. This observation, which cannot be explained by the dipole coupling effect alone, is most likely due to the electron contribution effect of Gd.

Our $NO + CH_4$–TPD results suggested that NO adsorbed at mid- and high-temperature sites were mostly converted to N_2 when CH_4 was co-adsorbed on the Gd–Pd catalyst. This implies that even at room temperature, CH_4 could be strongly adsorbed on the catalyst surface. Methane adsorption and reaction on Pd catalysts have been studied extensively in the past (14, 51–54). Our earlier studies using isotopic labeling experiments showed the formation of stable CH_x species on reduced Pd/TiO_2 surfaces (14). In the same study, we showed that while the metallic Pd sites were successful in activating methane by an initial hydrogen abstraction, the PdO sites led to complete combustion of methane (15).

Our present study provides additional evidence for the formation of surface CH_x species. The DRIFTS spectra taken under vacuum over $Gd–Pd/TiO_2$ catalysts following $NO + CH_4$ reaction showed the development of IR bands in the 2971–2850 cm^{-1} region, which correspond to –CH and $–CH_2$ vibrations (36, 55). The asymmetric and symmetric CH_3 deformation modes have characteristic bands around 1450 and 1350 cm^{-1}, respectively (46, 55). Although we observed bands in this region, the nitrogen-oxo species, which have their characteristic frequencies overlapping in

the same region, make the surface-species distinction more difficult. The existence of methyl species on the catalyst surface, however, remains as a distinct possibility. The TPD experiments which showed CO_2 formation after room-temperature adsorption of CH_4 provide further support for this possibility.

An interesting feature that emerged through the DRIFTS experiments was the formation of surface ammonia species. When the reduced catalyst surface was exposed to NO and CH_4 under conditions that gave complete NO conversion, bands that correspond to NH_3 coordinated to Lewis acid sites ($\sim$1180/1200 cm^{-1}) were observed. These bands were accompanied by features in the –NH stretching region (3242–3150 cm^{-1}). Interestingly these bands were never present over the oxidized catalyst, or under conditions where the catalyst was inactive for NO reduction. Also, in comparison to the Gd-free catalyst, the NH_3 formation seemed to be much more prominent over the Gd–Pd. When control experiments were performed to compare the steady-state NO reduction behavior of the reduced and oxidized Gd–Pd/TiO_2 catalyst at temperatures that corresponded to the temperatures at which *in situ* DRIFT spectra were obtained (300°C), we saw complete NO reduction over the reduced catalyst and very little reduction activity (less than 14%) over the oxidized catalyst. Another major difference was the high methane-combustion activity observed over the oxidized catalyst. These observations are consistent with our earlier results, which showed that Pd^0 sites were needed for the formation of CH_x species and that the oxide form of palladium led to complete combustion of methane (15). If we combine these findings with our present results, it appears that formation of CH_x species (i.e., abstraction of the first hydrogen) is a prerequisite for NH_3 formation. The fact that NH_3 formation, although in much smaller quantities, was observed over the TiO_2 support when NO and CH_4 were co-fed to the system, seems to suggest that the activation of CH_4 could also be accomplished through nitro–nitrito or monodentate nitrate species, which are abundant over the titania surface. This is consistent with earlier reports in the literature where CH_4 activation by adsorbed NO_2 was proposed for CH_4–NO reaction (20, 24, 25).

Another interesting finding from the present study is the apparent interaction between the surface-coordinated NH_3 species and linear Pd–NO species. DRIFTS experiments showed that disappearance of the Pd–NO species always coincided with the formation of surface ammonia species. This observation coupled with the steady-state reaction results lead us to suggest that adsorbed NH_3 could be an important player in the NO reduction scheme. The DRIFT experiments performed using sequential introduction of NO and NO + NH_3 flows over the reduced Gd–Pd/TiO_2 catalysts showed that as soon as NH_3 was introduced to the system, the Pd–NO species disappeared. This, coupled with the fact that nitrate species remained unchanged while Pd–NO species quickly disappeared, suggests that linearly adsorbed NO is the primary species that interacts with adsorbed NH_3 species. Steady-state reaction experiments performed over reduced Gd–Pd/TiO_2 catalysts that showed NH_3 to be a selective reducing agent over these catalysts, especially at lower temperatures, are in agreement with our spectroscopic findings (56).

There have been other reports in the literature where adsorbed NH_x was found to be an important surface species in the NO–CH_4–O_2 reaction. On Pd–H–Mordenite, Shimizu *et al.* observed using *in situ* IR that linearly adsorbed NO on Pd^{2+} species was reduced in a flow of CH_4 to form NH_4^+ which was adsorbed on Brønsted acid sites in zeolite. In addition, NH_4^+ species were found to react rapidly under the flow of NO or NO + O_2 to N_2 which suggested that Pd^{2+}–NO species and surface NH_4^+ species could be important surface species under reaction conditions. They proposed that the activation of CH_4 is derived from the dissociation of the C–H bond of CH_4 occurring over Pd^{2+} sites to form reactive species such as CH_x which subsequently interact with NO adspecies on Pd^{2+} to form NH_4^+ (57).

Although adsorbed NH_3 appears to be a key intermediate in the NO–CH_4 reaction, it is quite likely that the reaction scheme may involve multiple paths and multiple intermediates which may be in effect simultaneously. For example, the –CN and –NCO species have been reported to be important intermediates in the NO–CH_4–O_2 reaction over a Pd ion-exchanged zeolitic system (36, 57–59). These species are considered to be one of the surface intermediate species leading to N_2 and CO_2 formation. In our study, we did not detect these species, but the formation of C–N bonds as part of the reaction network seems quite plausible. It is also conceivable that while adsorbed NH_3 acts as a reducing agent "formed *in situ*," direct reduction by CH_x through a nitro- or nitrosomethane species also remains as a possibility. However, the present findings seem to suggest that NO oxidation to NO_2 does not have to be the only route for NO reduction over the Pd/TiO_2 catalysts.

CONCLUSIONS

In situ DRIFTS studies, coupled with TPD experiments performed in this study, suggest the NO species linearly adsorbed on Pd sites to be the major surface species under the reaction conditions. At lower temperatures, bridged/bidentate nitrate and monodentate nitrate are formed on the support and transformed to other compounds such as nitro, nitrito, and Pd–NO. There is strong evidence that methane and NO competitively adsorb on the surface even at room temperature. The Pd^0 sites are essential for dissociative adsorption of methane. Under conditions where the catalyst is fully active for NO reduction, NH_3 was seen to adsorb molecularly on Lewis acid sites. It appears that hydrogen abstraction from methane is a prerequisite for NH_3 formation. NH_x species are

believed to act as a reducing agent for reduction of adsorbed NO, although direct interaction of nitro/nitroso species with surface CH_x remains a possibility. The lanthanide elements are found to change the catalytic chemistry significantly. We suspect that the primary function of the lanthanide dopants, which are highly electropositive, is to increase the electron density around the Pd sites and to stabilize them in a reduced state. It is also possible that Gd helps control the crystal growth of the support and/or the palladium particles, making the active metal more readily accessible. Both of these functions may be in effect in the Gd–Pd/TiO_2 catalysts where the addition of Gd is seen to increase the oxygen resistance of the catalysts significantly in NO–CH_4 reaction.

ACKNOWLEDGMENTS

The financial contributions from the National Science Foundation and the Ohio Coal Development Office are gratefully acknowledged.

REFERENCES

1. Li, Y., and Armor, J. N., *Appl. Catal. B* **1**, L31 (1992).
2. Li, Y., Battavio, P. J., and Armor, J. N., *J. Catal.* **142**, 561 (1993).
3. Li, Y., and Armor, J. N., *Appl. Catal. B* **2**, 239 (1993).
4. Nishizaka, Y., and Misono, M., *Chem. Lett.* 1295 (1993).
5. Nishizaka, Y., and Misono, M., *Chem. Lett.* 2237 (1994).
6. Misono, M., Hirao, Y., and Yokoyama, C., *Catal. Today* **38**, 157 (1997).
7. Zhang, X., Walter, A. B., and Vannice, M. A., *Appl. Catal. B* **4**, 237 (1994).
8. Zhang, X., Walter, A. B., and Vannice, M. A., *J. Catal.* **155**, 290 (1995).
9. Cowan, A. D., Dümpelmann, R., and Cant, N. W., *J. Catal.* **151**, 356 (1995).
10. Burch, R., and Ramli, A., *Appl. Catal. B* **15**, 49 (1998).
11. Burch, R., and Ramli, A., *Appl. Catal. B* **15**, 63 (1998).
12. Ueda, A., Nakao, T., Azuma, M., and Kobayashi, T., *Catal. Today* **45**, 135 (1998).
13. Kumthekar, M. W., and Ozkan, U. S., *J. Catal.* **171**, 45 (1997).
14. Kumthekar, M. W., and Ozkan, U. S., *J. Catal.* **171**, 54 (1997).
15. Ozkan, U. S., Kumthekar, M. W., and Karakas, G., *J. Catal.* **171**, 67 (1997).
16. Kumthekar, M. W., and Ozkan, U. S., *Catal. Today* **35**, 107 (1997).
17. Mitome, J., Karakas, G., Bryan, K. A., and Ozkan, U. S., *Catal. Today* **42**, 3 (1998).
18. Mitome, J., Aceves, E., and Ozkan, U. S., *Catal. Today* **53**, 597 (1999).
19. Li, Y., and Armor, J. N., *J. Catal.* **150**, 388 (1994).
20. Lukyanov, D. B., Lombardo, E. A., Sill, G. A., d'Itri, J. L., and Hall, W. K., *J. Catal.* **163**, 447 (1996).
21. Kato, H., Yokoyama, C., and Misono, M., *Catal. Today* **45**, 93 (1998).
22. Kato, H., Yokoyama, C., and Misono, M., *Catal. Lett.* **47**, 189 (1997).
23. Lobree, L. J., Aylor, A. W., Reimer, J. A., and Bell, A. T., *J. Catal.* **169**, 188 (1997).
24. Aylor, A. W., Lobree, L. J., Reimer, J. A., and Bell, A. T., *J. Catal.* **170**, 390 (1997).
25. Sun, T., Fokema, M. D., and Ying, J. Y., *Catal. Today* **33**, 251 (1997).
26. Lombardo, E. A., Sill, G. A., d'Itri, J. L., and Hall, W. K., *J. Catal.* **173**, 440 (1998).
27. Karakas, G., Mitome-Watson, J., and Ozkan, U. S., *Catal. Comm.* **3**, 199 (2002).
28. Sharpe, R. G., and Bowker, M., *Surf. Sci.* **360**, 21 (1996).
29. Raval, R., Harrison, M. A., Haq, S., and King, D. A., *Surf. Sci.* **294**, 10 (1993).
30. Rodriguez, N. M., Oh, S. G., Dalla-Betta, R. A., and Baker, R. T. K., *J. Catal.* **157**, 676 (1995).
31. Farrauto, R. J., Hobson, M. C., Kennelly, T., and Waremann, E. M., *Appl. Catal. A* **81**, 227 (1992).
32. Hadjiivanov, K., Bushev, V., Kantcheva, M., and Klissurski, D., *Langmuir* **10**, 464 (1994).
33. Huang, S.-J., Walters, A. B., and Vannice, M. A., *Appl. Catal. B* **26**, 101 (2000).
34. Davydov, A. A., "Infrared Spectroscopy of Adsorbed Species on the Surface of Transition Metal Oxides." Wiley, 1990.
35. Hadijivanov, K., and Knozinger, H., *Phys. Chem. Chem. Phys.* **2**, 2803 (2000).
36. Captain, D. K., and Amiridis, M. D., *J. Catal.* **184**, 377 (1999).
37. Chi, Y., and Chuang, S. C., *J. Phys. Chem. B* **104**, 4673 (2000).
38. Hoost, T. E., Otto, K., and Laframboise, K. A., *J. Catal.* **155**, 303 (1995).
39. Solomun, T., *J. Electroanal. Chem.* **199**, 443 (1986).
40. Moriki, S., Inoue, Y., Miyazaki, E., and Yasumori, I., *J. Chem. Soc., Faraday Trans.* **78**, 171 (1982).
41. Grill, C. M., and Gonzalez, R. D., *J. Phys. Chem.* **84**, 878 (1980).
42. Xu, X., Chen, P., and Goodman, D. W., *J. Phys. Chem.* **98**, 9242 (1994).
43. Wickham, D. T., Banse, B. A., and Koel, B. E., *Surf. Sci.* **243**, 83 (1991).
44. Nyberg, C., and Uvdal, P., *Surf. Sci.* **250**, 42 (1991).
45. Almusaiteer, K., and Chuang, S. S. C., *J. Catal.* **184**, 189 (1999).
46. McGee, K. C., Driessen, M. D., and Grassian, V. H., *J. Catal.* **159**, 69 (1996).
47. Finocchio, E., Busca, G., Lorenzelli, V., and Willey, R. J., *J. Catal.* **151**, 204 (1995).
48. Ramis, G., *Appl. Catal.* **64**, 243 (1990).
49. Figoli, N. S., L'Argentiere, P. C., Arcoya, A., and Seoane, X. L., *J. Catal.* **155**, 95 (1995).
50. Dutta, P. K., Ginwalla, A., Hogg, B., Patton, B. R., Chwieroth, B., Liang, Z., Gouma, P., Mills, M., and Akbar, S., *J. Phys. Chem. B* **103**, 4412 (1999).
51. Baldwin, T. R., and Burch, R., *Appl. Catal.* **66**, 337 (1990).
52. Hicks, R. F., Qi, H., Young, L., and Lee, R. G., *J. Catal.* **122**, 280 (1990).
53. Huff, M., and Schmidt, L. D., *Catal. Today* **21**, 443 (1994).
54. Konig, D., Weber, W. H., Poindexter, B. D., McBride, J. R., Graham, G. W., and Otto, K., *Catal. Lett.* **29**, 329 (1994).
55. Busca, G., Lamotte, J., Lavalley, J., and Lorenzelli, V., *J. Am. Chem. Soc.* **109**, 5197 (1987).
56. Watson, J. M., and Ozkan, U. S., *J. Mol. Catal.,* in press.
57. Shimizu, K., Okada, F., Nakamura, Y., Satsuma, A., and Hattori, T., *J. Catal.* **195**, 151 (2000).
58. Lobree, L. J., Aylor, A. W., Reimer, J. A., and Bell, A. T., *J. Catal.* **181**, 189 (1999).
59. Bamwenda, G. R., Ogata, A., Obuchi, A., Takahashi, H., and Mizuno, K., *React. Kinet. Catal. Lett.* **56**, 311 (1995).